Advanced Drug Delivery Reviews 143 (2019) 161–176

Contents lists available at ScienceDirect

Advanced Drug Delivery Reviews

journal homepage: www.elsevier.com/locate/addr

Aggregation-induced emission (AIE) fluorophores as imaging tools to trace the biological fate of nano-based drug delivery systems

Yufei Wang [a,b], Yuxuan Zhang [a,b], Jinjin Wang [a,b], Xing-Jie Liang [a,b,*]

[a] CAS Center for Excellence in Nanoscience, CAS Key Laboratory for Biomedical Effects of Nanomaterials and Nanosafety, Chinese Academy of Sciences, National Center for Nanoscience and Technology of China, Beijing, 100190, China
[b] University of Chinese Academy of Sciences, Beijing, 100049, China

ARTICLE INFO

Article history:
Received 25 August 2018
Received in revised form 18 October 2018
Accepted 3 December 2018
Available online 6 December 2018

Keywords:
Aggregation-induced emission
Bioimaging tools
Nano-based drug delivery system
In vitro
In vivo

ABSTRACT

The vigorous development of nanotechnology has been accompanied by an equally strong interest and research efforts in nano-based drug delivery systems (NDDSs). However, only a few NDDSs have been translated into clinic thus far. One of the important hurdles is the lack of tools to comprehensively and directly trace the biological fate of NDDSs. Recently, aggregation-induced emission (AIE) fluorophores have emerged as attractive bioimaging tools due to flexible controllability, negligible toxicity and superior photostability. Herein, we recapitulate the current advances in the application of AIE fluorophores to monitor NDDSs both *in vitro* and *in vivo*. Particularly, we discuss the cellular fates of self-indicating and stimuli-responsive NDDSs with AIE fluorophores. Moreover, we highlight the *in vivo* application of AIE agents on the long-term tracking of therapeutics and the multi-modal monitoring of diagnostics in NDDSs. Challenges and opportunities in AIE-guided exploration of NDDSs are also discussed in detail.

Contents

1. Introduction

Over the past decades, rapid development of nanotechnology has transformed many areas of biomedical research, including tissue engineering, pharmaceutical discovery and disease diagnosis [1–6]. Notably,

* Correspondence author at: CAS Center for Excellence in Nanoscience, CAS Key Laboratory for Biomedical Effects of Nanomaterials and Nanosafety, Chinese Academy of Sciences, National Center for Nanoscience and Technology of China, Beijing, 100190, China.
E-mail address: liangxj@nanoctr.cn (X.-J. Liang).

https://doi.org/10.1016/j.addr.2018.12.004
0169-409X/

there has been a remarkable surge in the development and exploitation of nano-based drug delivery systems (NDDSs). For instance, in 1995, Doxil®, the first anticancer NDDS, was approved by the US Food and Drug Administration (FDA), and became a blockbuster oncotherapy [7]. Ten years later, the first protein-based NDDS, termed Abraxane®, got approval by the FDA. This albumin-coated paclitaxel delivery system has been widely utilized in oncological treatment, especially for breast cancer and pancreatic cancer [8]. Recently, in August 2018, Onpattro™, the FDA-approved lipid nanocomplex, became the first small interfering ribonucleic acid (siRNA) NDDS in the world [9]. Over the years, many types of NDDSs, such as those based on nanocrystals, micelles, nanoparticles, liposomes and nanoemulsions, became available to patients in preclinical and clinical trials.

Unlike traditional pharmaceuticals, NDDSs comprise an exquisite assembly of organic/inorganic nanomaterials and bioactive agents (chemical compounds, nucleotide fragments, peptides, *etc.*), translating into unique advantages. Firstly, the delivery of hydrophobic pharmaceuticals *via* NDDSs could enhance the solubility, leading to a sharp elevation of drug loading and bioavailability [4,10,11]. Secondly, NDDSs could perform targeted delivery of therapeutic agents. The main mechanisms can be concluded as active and passive targeting effects. After delicate surface modification of ligands (antibodies, peptides, aptamers, *etc.*), NDDSs can actively accumulate in biotargets through specific recognition between ligands and substrates [12–14]. In addition, as for the passive targeting effect, preferential tumor accumulation could be realized because of the enhanced permeability and retention (EPR) effect [15–17]. Both of these targeting actions – active and passive – can improve therapeutic effects and reduce adverse reactions in patients. Furthermore, the emergence of multi-functional NDDSs enables simultaneous diagnosis and therapy, resulting in timely and accurate disease control at the early stages [18,19]. Moreover, NDDSs may bring out improvements of pharmacokinetic (PK) properties, such as prolonged blood circulation and controllable biodistribution, which can benefit patients from lower dosages and longer dosing intervals [20–22]. Hence, it is possible for tailored NDDSs to be designed for the prevention, diagnosis and treatment of many different diseases.

The research and development of NDDSs attract global attention. The National Cancer Institute, part of the National Institutes of Health in the US, carried on an annual investment about $150 million for exploiting new NDDSs [23]. Also, the European Union proposed "the European Commission's Sixth Framework Programme" for nanomedicine and €650 million has been invested for preclinical and clinical trials [24]. However, only a few of such systems have been translated from benchside to bedside. Up to 2014, just 175 nanodrug products were approved by the FDA and the European Medicines Agency [25]. This disproportionally low-efficiency clinical transition might result from insufficient PK studies of NDDSs. Indeed, the absorption, distribution, metabolism, excretion and toxicity (ADMET) properties of NDDSs still remain elusive both *in vitro* and *in vivo* because conventional PK methods are not always suitable for investigating NDDSs. For instance, chromatographic detection, such as gas chromatography and high-performance liquid chromatography, performs high sensitivity and superb isolation efficacy but lacks the appropriate qualitative capability that is needed for analyzing multi-component living samples [26]. Furthermore, capillary electrophoresis relies on very small sample volumes so it is prone to cause low signal stability and poor sensitivity [27]. In addition, while immunoassays have high specificity and superior sensitivity, they can fail in a large-scale screening due to sophisticated operation and associated high cost [28]. More importantly, these analytical methods could only provide indirect measurements instead of direct visualization. Given to the fact that NDDSs structurally and functionally differ from traditional pharmaceuticals, it is necessary to implement dynamic and real-time visualization of nanocarriers and payloads. Thus, there still exists a need to develop imaging methods for exploration of NDDSs' biological fate.

In the past few years, the growing interest in monitoring the biological fate of NDDSs with diverse imaging tools has resulted in several important developments. In the search for better imaging quality in living systems, scientists are inclined to exploit fluorescent agents [29,30]. Notably, the team of Tang reported novel fluorophores with aggregation-induced emission (AIE) properties [31]. When reaching a high local concentration in solution and forming aggregates, both conventional fluorescein-based fluorophores and novel fluorescent nanomaterials are likely to suffer strong π-π stack, inducing a huge drop in fluorescence intensity in the process called "aggregation-caused quenching" (ACQ) [32,33]. On the other hand, AIE luminescent materials – or luminogens – emit stronger fluorescence when forming aggregates. Other properties of these fluorophores include flexible controllability, excellent photostability, high sensitivity and high selectivity [34].

Herein, we review the recent advances of the application of AIE fluorophores in both *in vivo* and *in vitro* imaging of NDDSs (Fig. 1). From the perspective of the *in vitro* fate, we describe AIE-guided cellular observations of both self-indicating and stimuli-responsive NDDSs. Concerning the *in vivo* fate, we highlight the long-term imaging of therapeutics and the multi-modal tracking of diagnostics in AIE-based NDDSs. Finally, potential obstacles and future perspectives of AIE-based biological imaging of NDDSs are also discussed.

2. Fundamentals of exploring the biological fate of NDDSs using AIE fluorophores

Since the discovery of AIE effects in 2001, great efforts have been made to utilize AIE-active materials in biological research. In this section, a brief overview of the development of AIE fluorophores is provided. Additionally, the properties and advantages of AIE-guided NDDS biological explorations are also discussed.

2.1. Discovery and development of AIE fluorophores

Numerous organic and nanomaterial-based fluorophores possess excellent fluorescent properties when dispersed in solution. However, aggregation of these materials is likely to result in fluorescent quenching due to the ACQ effect, which is largely responsible for non-radiative energy transfer induced by strong π-π stack. AIE agents, on the other hand, exhibit weak or no fluorescence in dispersion but emit strong fluorescence signals upon formation of aggregates (Fig. 2) [33,35–37]. Research on AIE phenomenon has gradually gained much popularity. From the Web of Science Database, the annual number of publications with the subject of AIE has exceeded 1000 since 2016. The inception of AIE fluorophores actually dates back to 2001 when Tang's group observed unusual fluorescence emission from silole molecules in different water-ethanol solutions [31]. When dispersing in ethanol and other preferred solvents, silole molecules are non-emissive because of nonradiative decay. However, in poor solvents like water, they may form aggregates, resulting in radiative decay and strong fluorescent emission. In water-ethanol mixed solution, as the fraction of water was elevated to 90%, the photoluminescence quantum yield of silole molecules exhibits a remarkable rise to 0.21, which is 333-times higher than that in ethanol. This fluorescence enhancement is due to the AIE phenomenon, which mechanism is largely attributed to the restriction of intramolecular motion (RIM). It is well accepted that the RIM process mainly includes the restriction of intramolecular rotation (RIR) and the restriction of intramolecular vibration (RIV) [38,39]. As for silole molecules, when dispersing in good solvents, the phenyl peripheries could perform free rotation around the central silole core. Once forming closely-packed aggregates, they undergo the RIR process, and the resulting radiative decay triggers strong excimer fluorescence. Besides, in shell-shaped molecules, such as 10,10′,11,11′-tetrahydro-5,5′-bidibenzo[a,d][7]annulenylidene (THBA), the RIV mechanism is the main cause of the AIE phenomenon [40]. The flexible phenyl rings of THBA exhibit dynamic vibration in solution. On the aggregate state,

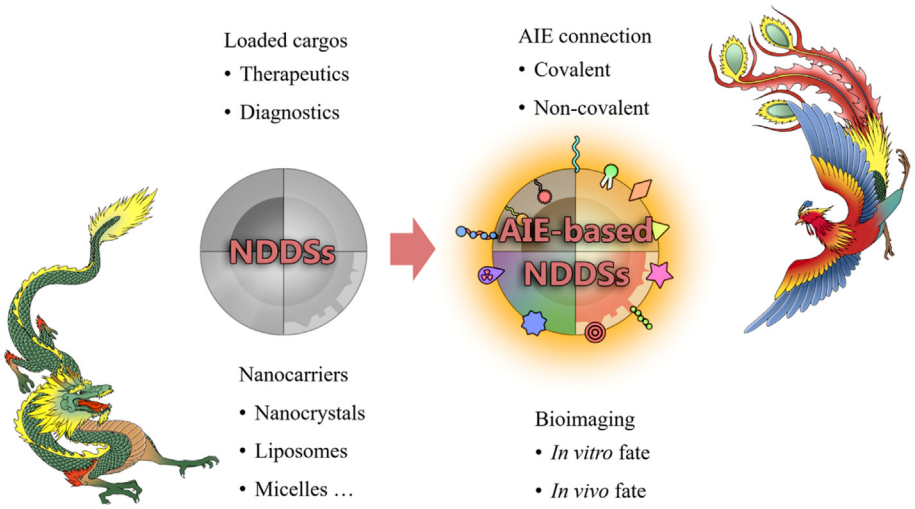

Fig. 1. A schematic representation of AIE-based NDDSs. The diversity of NDDSs mainly stems from loaded cargos, and nanocarriers. AIE fluorophores can be introduced into NDDSs through covalent or non-covalent connections. Then, the behaviors of nanocarriers or integral NDDSs (*in vitro* and *in vivo* fate) can be traced by the fluorescent signals of AIE fluorophores.

its intramolecular vibration is considerably restricted due to the steric hindrance. Thus, the radiative decay pathway is opened and allows THBA highly emissive. Apart from the RIM mechanism, J-aggregate formation, conformational planarization, and excited-state intramolecular proton transfer (ESIPT) also account for the AIE behavior [34,39,41]. Most organic fluorophores with coplanar structures are prone to form H-aggregates in the face-to-face parallel alignment due to strong π-π stack, which results in fluorescence quenching. However, if the intermolecular distance is extended to form slanted stacks as J-aggregates, fluorophores may render enhanced emissions. It is evident that J-aggregate formation can be observed in several AIE molecules [42–44]. Besides, conformational planarization relies on twisted-coplanar structural changes to preclude π-π stack and activate radiative decay [45]. Moreover, ESIPT, a process of energy relaxation *via* keto-enol tautomerization, is also reported in many AIE behaviors [46–48].

As a result of their tunable fluorescent properties, AIE agents have found increasing use in biological research. The main four AIE backbone structures and examples of their applications are shown in Fig. 3 and Table 1. Most AIE molecules comprise polycyclic and heteroaromatic structures. Tetraphenylene (TPE) is one of the most widely used AIE agents in biological studies. Upon aggregation of these molecules, steric hindrance of the peripheral phenyl rings leads to nonplanar and propeller-like conformation, which can leads to the RIR process and trigger the AIE effect [49]. Due to its facile synthesis, TPE can be employed as a flexible building block in the construction of AIE-based nanostructures for bioimaging. Other AIE backbones include cyano-substituted stilbene, triphenylamine (TPA) derivatives and tetraphenylsilole. Park et al. reported AIE-exhibiting cyano-substituted stilbene agents (CN-MBE) in 2002 [45]. When forming aggregates, CN-MBE could emit almost 700-time stronger fluorescent signals than in dilute solution. The main mechanisms of their AIE properties can be ascribed to coplanarization and J-aggregate formation. NPAPF, one of cyano-substituted stilbene molecules, has been employed in the studying of targeted cell imaging and bio-nano interactions [50]. TPA shows the ACQ effect in the aggregation state. However, through exquisite introduction of peripheral groups around TPA cores, researchers synthesized AIE-exhibiting TPA derivatives [51]. These derivatives can possess broad-band fluorescence emission and are suitable for the visualization of drug delivery and pathophysiological diagnosis. Tang's team has contributed a lot in the optimization design of tetraphenylsilole-based AIE molecules [52–54]. They synthesized a series of efficient AIE molecules by changing silicon substituent groups. These

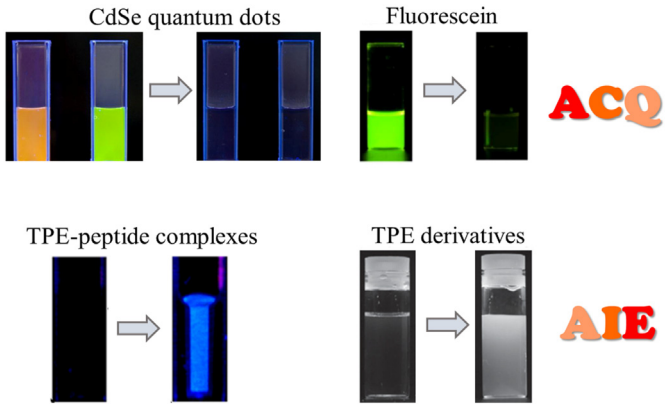

Fig. 2. Fluorescence emission changes resulting from solution-aggregation transitions due to the ACQ and AIE effects. Top panel: CdSe quantum dots of different sizes and fluorescein undergo fluorescence quenching in the aggregated state. Lower panel: tetraphenylene (TPE) derivatives and complexes exhibit strong fluorescence emission when forming aggregates. Adapted with permission from [33,35–37]. Copyright 2010 Elsevier, 2016 Royal Society of Chemistry, 2012 American Chemical Society and 2015 John Wiley and Sons, respectively.

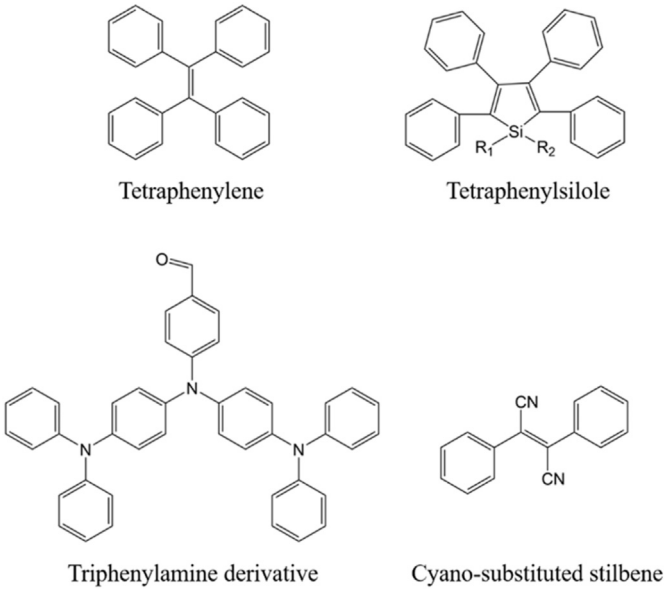

Fig. 3. The most prominent AIE backbone structures commonly used in biological research.

Table 1
The main biological applications of AIE-based nanostructures.

Classification	AIE backbone structure	Nano structure	λ_{ex} (nm)	λ_{em} (nm)	Use type	Biological application	Reference
Tetraphenylene (TPE)	TPE-MI	TPE-MI-peptide complexes	355	445–500	*In vitro*	Evaluation of proteostasis in Huntington's disease	[55]
	TPE-In	TR4@siRNA@Tf nanocomplexes	330	~460	*In vitro*	Intracellular gene delivery and evaluation of transfection efficiency	[56]
	TPEDC	T-TPEDC nanodots	800	590–630	*In vitro/in vivo*	Photodynamic therapy for precise blood vessel closure	[57]
	TPE-TETRAD	TPE-TETRAD saponin nanoparticles	488	600–750	*In vitro*	Ultra-fast intracellular delivery	[58]
	TPEE-Rho	TPEE-Rho dots	530	~600	*In vitro/in vivo*	Long-term imaging of tumor growth in mice	[59]
	TPECM	TPECM-peptide complexes	405	560	*In vitro*	Targeted photodynamic ablation of cancer cells	[60]
	TPE	TR4 nanofibers	405	505	*In vitro*	Detection of the integrity of cell membrane	[61]
	TPE-CHO	DOX-loaded NDDS	405	450	*In vitro*	Intracellular delivery of doxorubicin in pH-responsive NDDS	[62]
	TPE	Biosensor with TPE and protoporphyrin IX	405	~450	*In vitro/in vivo*	Photodynamic therapy and evaluation of matrix metalloproteinase-2 expression	[63]
Cyano-substituted stilbene	NPAPF	BOSA–NPAPF nanoparticles	405	650	*In vitro*	Targeted cancer cell imaging	[64]
	NPAPF	Nanoparticles	405	420–480	*In vitro*	Investigation of the influence of surface modification on nanoparticle-cell interactions	[65]
Triphenylamine (TPA) derivatives	CAPP	CAPP saponin nanoparticles	488	600–700	*In vitro*	Ultra-fast intracellular delivery	[58]
	TQ-BPN	TQ-BPN nanodots	635	~810	*In vitro/in vivo*	Angiography of damaged blood brain barrier in mice	[66]
	TPA-BI	TPA-BI nanoaggregations	840	450–550	*In vitro/in vivo*	Imaging of lipid droplets	[67]
Tetraphenylsilole	Net-TPS-NCS	Net-TPS-PEI-DMA nanoparticles	405	505	*In vitro*	pH-responsive imaging of targeted cancer cells	[68]
	BATPS	TPS-2cRGD complexes	405	505–525	*In vitro*	Quantitative imaging of integrin $\alpha_v\beta_3$ in cancer cells	[69]

tetraphenylsilole-based AIE molecules can be easily constructed into multifunctional nanostructures for the qualitative and quantitative detection of cancer cells and biomolecules.

2.2. AIE-guided biological evaluation of NDDSs

The ground-breaking development of NDDSs has attracted worldwide attention. Many critical differences between traditional drugs and NDDSs need to be mentioned. Firstly, in terms of structure and components, traditional pharmaceutical formulations mostly consist of a single drug and biodegradable excipients, whereas NDDSs can be rather described as "intricate combinations". The bioactive components of NDDSs, such as chemical compounds, peptides, antibodies and nucleotide fractions, are usually encapsulated into nanocarriers through non-covalent interactions [70–73]. Another common strategy is to covalently conjugate bioactive agents with nanocarriers [74–76]. Thus, different from free drugs, NDDSs can perform precise and controllable release of bioactive cargos due to their intricate nanostructures. Secondly, in terms of clinical function, traditional pharmaceuticals mainly perform a single therapeutic function, whereas NDDSs can be multifunctionalized to achieve disease prevention, diagnosis and treatment at the same time. Notably, these structural and functional differences could induce great changes in biological behaviors and ADMET properties. For example, upon entering a living body NDDSs may undergo opsonization in the bloodstream. Some of these structures can be removed by the reticuloendothelial system (RES), while the rest might accumulate in specific tissues and organs *via* passive/active targeting. At the cellular level, following surface recognition and endocytosis, NDDSs might undergo endo−/lysosomal escape in the cell and release bioactive agents to reach subcellular targets. Finally, a proportion of NDDSs and their metabolites would be excreted from the cell and body. The general PK and pharmacodynamic (PD) analysis of NDDSs has been previously investigated [77–83]. However, there still remains the urgent need for realizing direct, dynamic and specific observations of the fate of NDDSs in biological systems.

Recently, several researcher groups have been able to track *in vitro* and *in vivo* fate of NDDSs by applying various imaging tools such as computed tomography (CT), positron emission tomography (PET), single photon emission computed tomography (SPECT), magnetic resonance imaging (MRI) and fluorescence imaging [84–87]. Among these imaging tools, CT, PET and SPECT are particularly suitable to analyze metabolic processes, but low resolution, insufficient sensitivity and complicated operation restrict their further application to monitor the fate of NDDSs [88–90]. The bottlenecks in the application of MRI, on the other hand, include low sensitivity, long scanning time and metal-induced perturbations [91]. In contrast, high sensitivity, high resolution and excellent imaging quality make fluorescence imaging a promising tool for biological studies of NDDSs. The efficacy of fluorescent agents is often the major determinant of imaging quality, and is thus the prerequisite in fluorescence imaging. Green fluorescent protein can exhibit stable signals but the troublesome transfection makes it less practical for multi-process monitoring of NDDSs, especially in low-pH environments [92]. As for small organic fluorophores, such as fluorescein isothiocyanate, rhodamine and cyanine dyes, their poor photostability, sophisticated synthesis and the ACQ effect are major obstacles that prevent their usage to visualize the activation, biodistribution and degradation of NDDSs [32,93]. Despite the high potential of the more recently developed fluorescence resonance energy transfer (FRET) fluorophores, their application is hindered by complicated molecular design, photobleaching and background interference [94,95]. In contrast, AIE luminogens have provided novel opportunities for bioimaging by virtue of facile synthesis and excellent biosafety [96–99]. More importantly, little loss of the fluorescence intensity can be observed during cell incubation and animal feeding, convincing the comparable photostability of AIE molecules [100–102]. NDDSs' biological explorations with different fluorophores (AIE, ACQ and FRET) are shown in Table 2. Through covalent and non-covalent connections, AIE fluorophores can be successfully integrated into diverse NDDSs. Due to the hydrophobicity of most AIE fluorophores, researchers could assemble them with amphiphilic polymers in solution [99]. Furthermore, researchers have also developed non-covalent connections *via* electrostatic interactions [103]. These physical fabrication methods seem simple but unstable in dynamic biosystems. Therefore, covalent connections are regarded as another common way to form AIE-based NDDSs. Direct covalent linkages rely on specific chemical groups such as carboxyl, hydroxyl, aldehyde, amino groups, and so on [61,62,104]. Besides, emulsion polymerization

Table 2
Comparison of AIE, ACQ and FRET and their biological explorations of NDDSs.

Type	Phenomenon	Photochemical mechanism	*In vitro* exploration of NDDSs			*In vivo* exploration of NDDSs		
			Fluorophores	Exploration	Reference	Fluorophores	Exploration	Reference
AIE	Weak or no emissions in solution while strong emissions in aggregates.	In aggregates, the restriction of intramolecular motion activates radiative decay pathway, resulting in enhanced fluorescence emissions.	TPE	Lysosomal escape and nuclear translocation of DOX	[105]	TPE derivatives	Multimodal imaging of fluorescent imaging, dark-field microscopy and computed tomography	[106]
			TPE	Cellular delivery and nuclear translocation of Tamoxifen	[107]	TPE	Long-term and multimodal imaging of fluorescent imaging and magnetic resonance imaging in rat liver	[108]
			Cyano-substituted stilbene	Mitochondrial delivery of DOX	[109]	TPE	Multimodal analysis of fluorescent imaging and inductively-coupled plasma mass spectrometry in blood brain barrier	[110]
ACQ	Strong emissions in solution while weak or no emissions in aggregates.	In aggregates, intermolecular π-π stack inhibits radiative decay and induced non-radiative relaxation, resulting in loss of fluorescence emissions.	*aza*-BODIPY (P2) and *aza*-BODIPY (P4) fluorophores	Size-dependent trans-monolayer transportation of nanoemulsions	[111]	*aza*-BODIPY (P2) and *aza*-BODIPY (P4) fluorophores	Size-dependent digestion of nanoemulsions in gastrointestinal tract through oral absorption	[111]
			aza-BODIPY (P2)	Evaluation of lipolysis kinetic parameters of lipid-based nanocarriers	[112]	*aza*-BODIPY (P2)	Preferential biodistribution of intravenous micelles in rat extremities and vital organs	[113]
FRET	The emission spectrum of a donor overlaps the excitation spectrum of a receptor. When they are close enough (<10 nm), the donor undergoes quenching but the receptor emits enhanced fluorescence.	Through long-range dipole-dipole coupling, energy transfer is processed in non-radiative way from the donor to the receptor.	The FRET pair of DOX and 7-hydroxycoumarin-3-carboxylate	Real-time monitoring of dual-drug release in cancer cells	[114]	The FRET pair of Cy7 and varying tail fluorophores	Influence of the hydrophobicity and miscibility of NDDSs' cargos on tumor accumulation	[115]
			The FRET pair of BODIPY and spiropyran	Quantitative visualization of drug release from micelles	[116]	The FRET pair of DiI and DiD	Formulation-dependent biodistribution of different micelles	[117]

and ring-opening metathesis polymerization are also employed [99]. Hence, after integrated into NDDSs, AIE agents could show up the movements and behaviors of carriers or the integral NDDSs. It is possible to obtain more targeted, complex, and comprehensive observations of NDDSs' travel through the cell, tissue/organ or the whole body, which can strongly facilitate the future development of NDDSs.

3. *In vitro* fate of NDDSs

To be successfully delivered into intracellular milieu and reach their subcellular targets, NDDSs need to overcome several barriers and undergo a series of cellular transports. After anchoring at cell surfaces, NDDSs need to pass through the plasma membrane *via* endocytosis and be sequestered into endo−/lysosomes. Most of NDDSs need to achieve endo−/lysosomal escape so that bioactive agents could be released into the cytosol and then transported to the organelles, nucleus, and other subcellular targets [118–120]. Obtaining dynamic visualization is therefore the prerequisite for better analysis of the *in vitro* fate of NDDSs. With the advantages of AIE luminogens, real-time monitoring of NDDSs *in vitro* behavior could be achieved. In this section, we mainly focus on the application of AIE agents in cellular observations of self-indicating and stimuli-responsive NDDSs.

3.1. Self-indicating NDDSs

To explore the cellular fate of NDDSs, fluorophores can be integrated into these systems to endow them with self-indicating property, providing new opportunities to directly monitor the uptake, activation, release, transport and exocytosis of NDDSs. Traditional monomolecular fluorophores such as 5-carboxyfluorescein, fluorescein isothiocyanate and dansyl chloride typically require complex synthesis. Therefore, there is still a need to exploit novel fluorescent markers with lower molecular weights, facile synthesis, flexible bioconjugation and high biocompatibility. In the recent years, AIE molecules have been introduced into NDDSs as self-indicating fluorescent labels. For example, Yu et al. prepared a metallacage nanoparticle (MNP) containing TPE fluorophores [121]. Within the tetragonal structure of MNPs, the researchers incorporated TPE as the vertices and the bioactive Pt(II) cargo as metal nodes. Additionally, they also introduced biotin into the “arms” or extensions of these MNPs to achieve biotin-mediated targeting to cancer cells. The closely-packed prism of these MNP structures largely restricted intramolecular ring rotation of TPE, leading to strong fluorescence emissions for bioimaging. The *in vitro* behavior of the MNPs was investigated in HeLa and HepG2 cancer cells which overexpress biotin receptors. After 0.5 h of incubation, a little fluorescence was observed, suggesting the incipient endocytosis of MNPs. When the incubation time increased to 2 h and 4 h, the green signals of MNPs co-localized with the nuclei. Thus, MNPs enabled the delivery of Pt(II) into the nuclei of the targeted cells to act as anticancer agents.

Apart from covalent conjugation, AIE agents can also be integrated into NDDSs through non-covalent, physical interactions. Using high-speed stirring and precipitation, Gao et al. prepared TPE-mixed paclitaxel (PTX) nanocrystals (PTX/TPE NCs) [122]. After incubating these NCs with KB and HT-29 cells for the indicated times (Fig. 4), the researchers labeled the cell membranes with DiI dyes to analyze the endocytosis, dissolution and exocytosis of PTX/TPE NCs. After 1 h of incubation, PTX/TPE NCs entered the cells as observed by the blue emission inside the cell membranes. As the incubation was prolonged to 3 h and 7 h, cellular blue signals of PTX/TPE NCs were firstly getting stronger but then began to weaken, which is attributed to the slow dissolution of PTX/TPE NCs. Additionally, to investigate the exocytosis, the researchers treated cells with PTX/TPE NCs for 3 h and incubated them in fresh

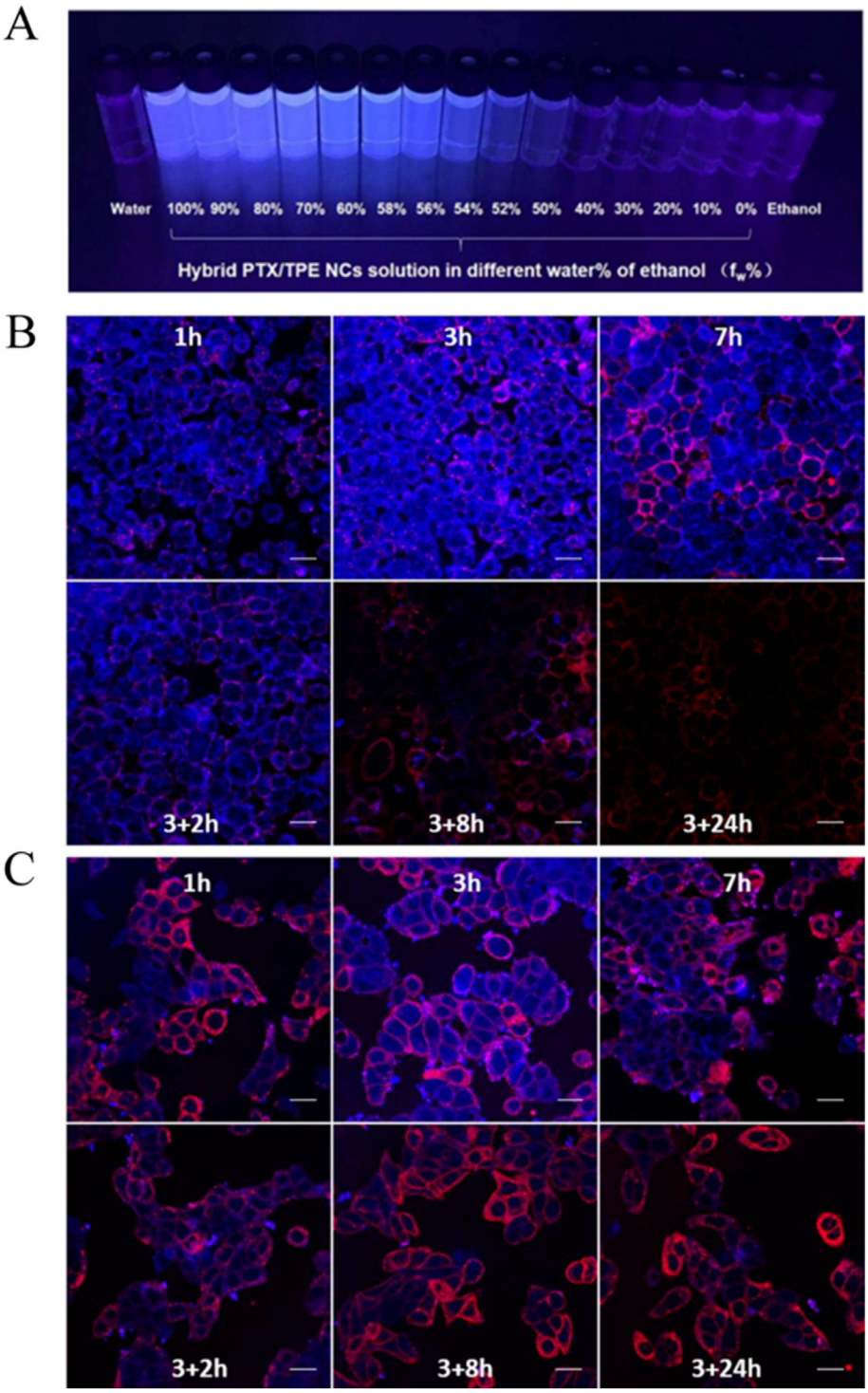

Fig. 4. Cellular observations of self-indicating PTX/TPE nanocrystals (NCs). (A) Different fluorescence emissions of PTX/TPE NCs in water-ethanol solvent mixtures. Confocal laser scanning microscopy (CLSM) images of KB cells (B) and HT-29 cells (C) co-cultured with PTX/TPE NCs for 1, 3, 7 h or another 2, 8, 24 h incubation with fresh medium after the 3-h treatment. (Blue: PTX/TPE NCs; Red: cell membranes; Scale bar: 20 μm). Adapted with permission from [122]. Copyright 2017 Elsevier.

medium for different times. The results verified that blue fluorescence signals appeared both in the cytosol and outside the cell membranes. Therefore, a portion of intracellular PTX/TPE NCs might remain in the cytoplasm while some might be translocated back to cell surfaces and the extracellular milieu.

In addition to drug delivery, AIE fluorophores can also be applied to visualize gene delivery *via* NDDSs. As shown in Fig. 5, the research team of Liang developed a self-indicating nanofiber containing plasmid DNA (pDNA) [123]. They used a TPE-based vector to encapsulate pDNA and finally prepared pDNA@TR4 nanofibers. The researchers were then able to track cellular behaviors through different fluorescence signals as the green emission of vectors and the red emission of Cy-5-labeled pDNA merged to be purple signals of pDNA@TR4 nanofibers. After 4 h of co-culture, pDNA@TR4 nanofibers were observed on the surface of HeLa cells, while at 24 h of incubation the purple fluorescence could be observed inside the cells, implying that pDNA@TR4 nanofibers entered into the cytosol. Meanwhile, some red signals appeared and showed little co-localization with the lysosomes, suggesting that a

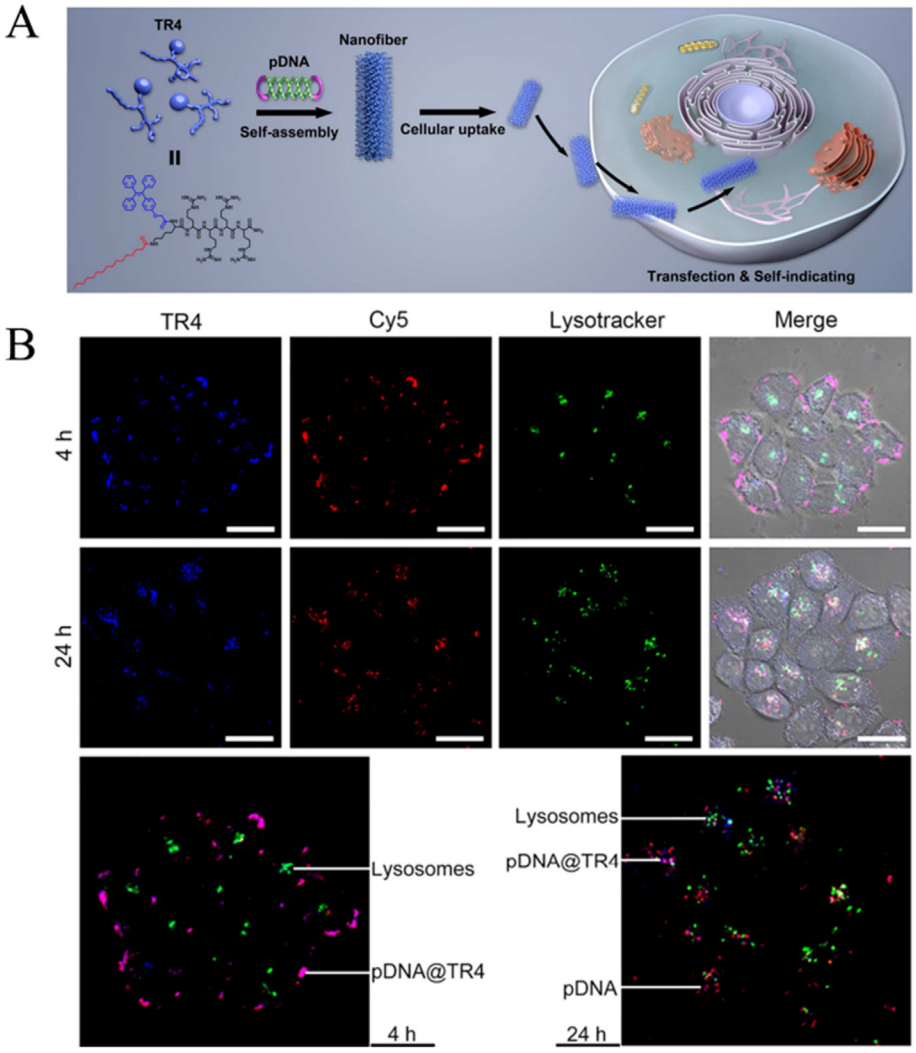

Fig. 5. Cellular observations of self-indicating pDNA@TR4 nanofibers containing TPE-based vectors. (A) TPE moieties were conjugated to TR4 vectors followed by plasmid DNA encapsulation to produce self-indicating nanofibers. The subcellular distribution could be observed due to the different fluorescence signals. (B) CLSM images of HeLa cells after the treatment with pDNA@TR4 for 4 h and 24 h. (Blue: TPE-conjugated TR4 vectors; Red: Cy5-labeled plasmid DNA; Green: lysosomes; Scale bar: 20 μm). Adapted with permission from [123]. Copyright 2017 American Chemical Society.

part of pDNA was detached from the pDNA@TR4 nanofibers and released from the lysosomes into the cytoplasm. With a better understanding of when and where pDNA gained liberation from the vectors, researchers could design tailored NDDSs for higher gene releasing and transfection efficiency.

3.2. Stimuli-responsive NDDSs

Unsatisfactory solubility, poor specificity and low bioavailability are the major obstacles in drug discovery with traditional pharmaceuticals [124]. NDDSs offer a potential solution to these problems. For example, stimuli-responsive NDDSs have gained great attention for their superior target specificity. When exposed to various stimuli (temperature, light, electric pulse, magnetic field, enzyme, pH, redox, *etc.*), they can react readily through specific changes in their structures and properties, finally triggering the release of bioactive agents. In 1978, Blumenthal's group found that the release ratio of neomycin-loaded liposomes at 44 °C was 100 times higher than that at 37 °C, which can be considered as the first stimuli-responsive NDDS [125]. Since then, researchers have taken enormous efforts to design stimuli-responsive NDDSs with high sensitivity, good stability and flexible controllability [126–129]. However, it is difficult to directly monitor intracellular changes of NDDSs with external stimuli. Fortunately, AIE fluorophores could perform these dynamic processes by their aggregation-induced fluorescent changes. Thus, relying on the "on/off switch" scenario of AIE fluorophores, *in vitro* fate of stimuli-responsive NDDSs can be monitored to obtain detailed information on drug-target interactions.

3.2.1. pH-responsive NDDSs

Upon entering the cytoplasm through endocytosis, NDDSs are prone to being engulfed into endo−/lysosomes, which triggers their degradation and deactivation of bioactive agents. Endosomes and lysosomes are rather acidic environments with pH 5–6.5 and 4–5, respectively, whereas the pH value of cytoplasm fluctuates between 6.8 and 7.4 [130]. This intracellular pH gradient can be an impactful tactic to design endo−/lysosomal escape for efficient drug releasing. So far, diverse pH-responsive NDDSs have been designed to afford controllable release of loaded cargos (pharmaceuticals, peptides, nucleotide fragmentations, *etc.*) [131–134].

To monitor the cellular fate of pH-responsive NDDSs in real-time, Xue et al. combined TPE-COOH and doxorubicin (DOX) through electrostatic interactions to thus finally construct AIE-based pH-responsive TPE-DOX nanoparticles (TD NPs) (Fig. 6) [103]. At neutral pH of 7.4, TPE agents in TD NPs showed a decreased emission due to the energy transfer toward DOX. Despite receiving extra energy from TPE, DOX in TD NPs did not produce strong red signals due to the intramolecular

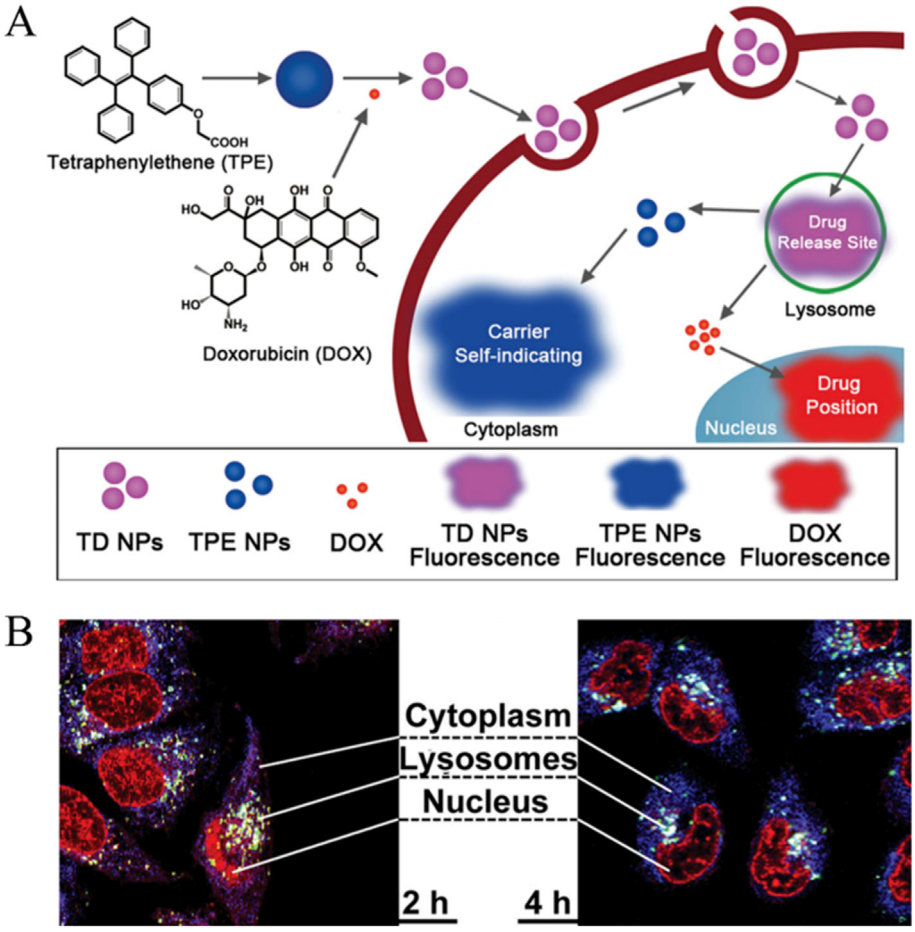

Fig. 6. Cellular tracing of pH-responsive TPE-DOX nanoparticles (TD NPs). (A) Changes in the fluorescence of TPE, DOX and complete TD NPs can elucidate the processes of endocytosis and intracellular breakdown of TD NPs. The different termini of DOX and TPE carriers could also be traced in cells. (B) CLSM images of MCF-7 cells incubated with TD NPs for 2 h and 4 h. (Blue: TPE carriers; Red: DOX cargo; Purple: TD NPs; Green: lysosomes). Adapted with permission from [103]. Copyright 2013 John Wiley and Sons.

"π-π stacking". Hence, the fluorescence emissions of TPE and DOX in TD NPs were both weakened at neutral pH. In contrast, with the exposure to acidic environments such as lysosomes, TD NPs could break up to release TPE carriers and DOX molecules, leading to acid-sensitive drug release and largely enhanced fluorescence signals of TPE and DOX. To further evaluate cellular behaviors of TD NPs, the research team incubated MCF-7s cells with these nanoparticles and compared their confocal laser scanning images. They found that after endocytosis TD NPs could be disassembled in response to the low pH in lysosomes. Finally, the red signals appeared in the nucleus, suggesting that DOX molecules were successfully transported into the nucleus, where the drug could exert its anticancer effects. In contrast, the TPE carriers largely stayed in the cytoplasm. Therefore, through analyzing the spatio-temporal distributions of different fluorescence signals, the researchers were able to monitor the breakdown of pH-sensitive NDDS structures and trace *in vitro* behaviors of bioactive agents and carriers. Additionally, the same research team also constructed TPE-DOX NDDSs with cleavable hydrazone bonds and prepared another pH-responsive NDDS termed THyD NPs [104]. In this work, THyD NPs showed weak or no fluorescence at neutral pH due to the ACQ effect, whereas in acidic lysosomes the hydrazone bonds were ruptured and the released DOX could emit strong red fluorescence. Hence, the researchers could monitor the "unpacking" process of THyD NPs. In MCF-7 cells incubated with THyD NPs, TPE and DOX showed no fluorescence at first, which demonstrates that THyD NPs were potentially taken up into cells and did not begin to hydrolyze. Afterwards, purple signals appeared in the lysosomes, suggesting that hydrazone bonds of THyD NPs broke in response to the drop in pH. Following the bond breaking event, the released DOX and TPE molecules showed strong and different fluorescence emissions. Similar to TD NPs, most DOX in THyD NPs was released and finally translocated into the nuclei, while the TPE carriers remained largely in the cytosol. Importantly, the researchers verified that although TD- and THyD-based NPs showed similar release behaviors in response to intracellular pH gradients, the rates of their release were very different. Thus, after 3 h of treatment with TD NPs, most DOX co-localized with lysosomes, but many red signals appeared in the nucleus. After 6 h, most DOX translocated into the nucleus, indicating the end of rapid drug release in TD NPs. On the other hand, in cells treated with THyD NPs, in the first 12 h of incubation, the intracellular distributions of DOX and TPE showed no sharp increases. After a 24-hour treatment, many DOX signals localized at perinuclear and nuclear sites. Hence, THyD NPs are characterized by a slower, sustained release of the cargo. These different release rates can be attributed to the underlying interactions between TPE and DOX. Compared with electrostatic forces, hydrazone bonds are stronger and less likely to disrupt, and thus THyD NPs showed a sustained release. Therefore, with the assistance of AIE molecules, it is possible to evaluate ADMET properties of different pH-sensitive NDDSs in detail.

3.2.2. Light-responsive NDDSs

With the advantages of non-invasiveness, spatial precision and remote control, light-responsive NDDSs, which undergo efficient and precise drug release when exposed to specific light irradiation, have gained much popularity [135–138]. Conventional strategies in light-triggered drug release rely on such processes as *trans-cis* isomerization, spiropyran-mero-cyanine isomerization, host-guest recognition and

dehybridization-hybridization transition [137,139–141]. Recently, several photosensitizers that are able to generate non-lethal amounts of reactive oxygen species (ROS) upon specific light exposure have been used in the construction of NDDSs to enhance the permeability of endo−/lysosomal membranes and facilitate the release of bioactive agents [142,143]. As many of AIE fluorophores can also induce ROS production, it is likely that such AIE agents can serve not only as fluorescent labels, but also as efficient photosensitizers for light-induced NDDS disassembly and drug release. For instance, Yuan et al. developed a light-responsive NDDS to elevate the delivery efficacy of DOX (Fig. 7) [144]. TPETP, a derivative of TPE, was conjugated to polyethylene glycol (PEG) chain *via* an ROS-sensitive thioketal (TK) linker. The amphiphilic TPETP-TK-PEG construct could encapsulate DOX to generate a AIE-NPs/DOX delivery system. As part of this system, both TPETP and DOX exhibited weak emissions because of mutual fluorescence quenching. Once exposed to light irradiation, the rapidly generated ROS could break the TK linkers, inducing the release of DOX, allowing both TPETP carriers and DOX compounds to exhibit strong fluorescence signals. The *in vitro* fate of AIE-NPs/DOX in DOX-resistant MDA-MB-231 cells was then investigated. In the absence of light irradiation, the red signals of TPETP carriers almost completely co-localized with the green ones of DOX in the lysosomes, implying that AIE-NPs/DOX were engulfed into lysosomes after endocytosis. Significantly, given to the fact that red emissions of DOX showed no obvious overlay with the nuclei, the researchers verified that the drug release was not initiated in the absence of light exposure. The AIE-NPs/DOX-treated cells were then irradiated with white light (0.1 W/cm^2, 2 min) and incubated in fresh medium for another 2 h. As a result, strong cyan signals, as the overlay of the blue emissions from the Hoechst reagent and the red emissions from DOX, appeared in the nucleus sites, implying that DOX was rapidly released from the lysosomes and diffused into the nucleus. Contrarily, the red signals of TPETP carriers were still dispersed in the cytosol, indicating that TPETP was not transported into the nucleus. Overall, it was possible to monitor the process of light-responsive breakdown of NDDS constructs and the subsequent lysosomal escape, and compare the intracellular distribution of both the cargo and carrier molecules.

Light-responsive NDDSs are utilized to deliver not only pharmaceuticals, but also nucleic acids to the desired target sites. For nucleotide-loaded NDDSs, the endo−/lysosomal entrapment and low-efficiency release become tough hurdles. Fortunately, it has been shown that light-

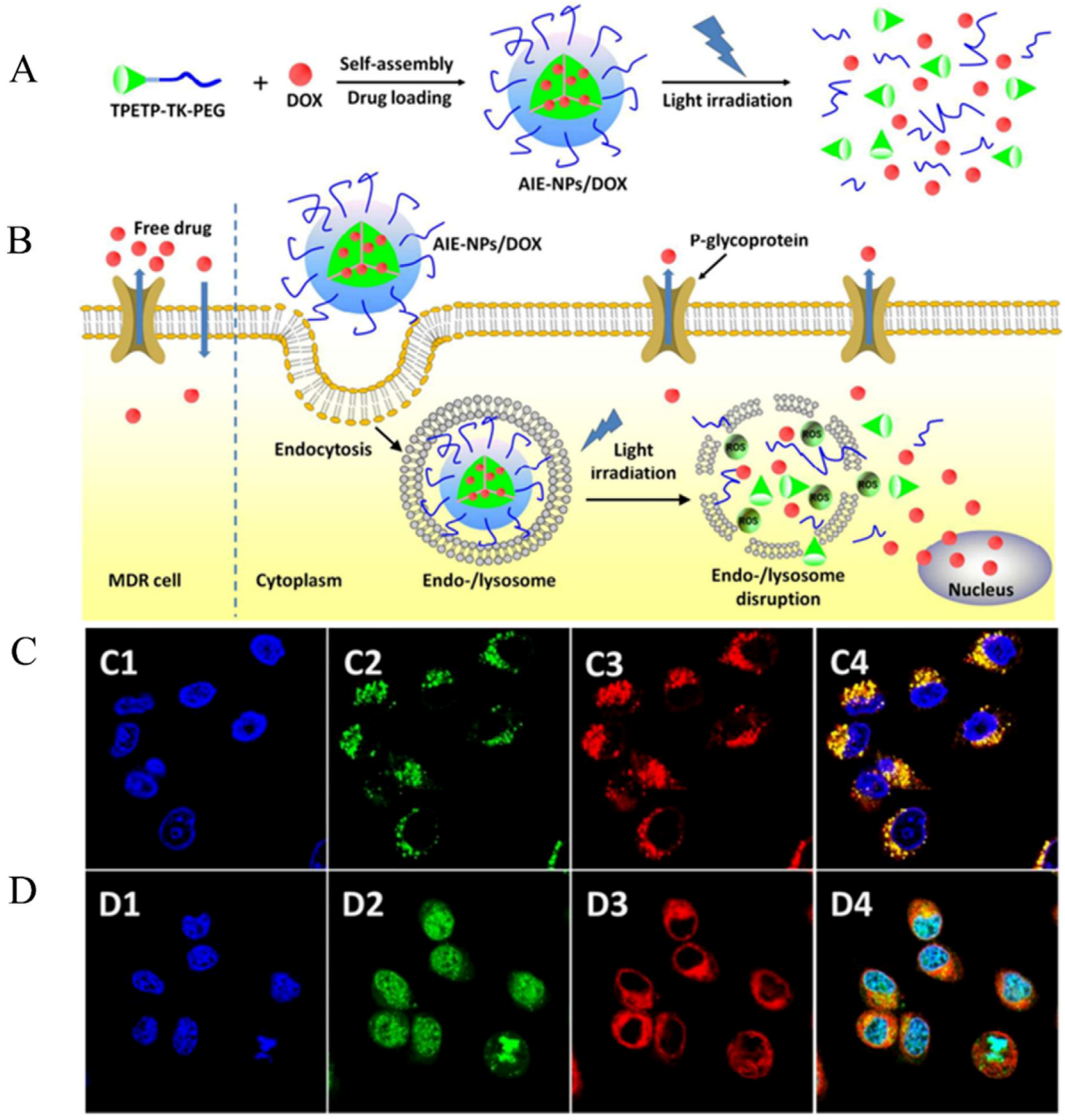

Fig. 7. *In vitro* tracking of the light-responsive AIE-NPs/DOX system. (A) A dual-function polymer, consisting of TPETP and PEG tethered through a light-sensitive TK linker, and DOX were self-assembled to construct AIE-NPs/DOX nanosystems that could undergo light-induced drug release. (B) CLSM observations of DOX-resistant MDA-MB-231 cells treated with AIE-NPs/DOX for 2 h and incubated for another 2 h in fresh medium. (Blue: cell nuclei; Green: DOX; Red: TPETP-based carriers). Adapted with permission from [144]. Copyright 2016 Royal Society of Chemistry.

triggered ROS-mediated disruption of NDDSs can promote endo−/lysosomal escape and facilitate the unpacking and translocation of DNA fragments [145]. The research team of Liu synthesized a light-responsive DNA-encapsulating nanosystem, termed S-NPs/DNA [146]. Similar to the aforementioned AIE NPs/DOX, another TPE derivative–TPECM, served both as a fluorescent label and photosensitizer. S-NPs nanovectors were generated by tethering TPECM and oligoethylenimine (OEI) through ROS-sensitive aminoacrylate linkers [147]. Due to excellent DNA-binding properties of OEI, S-NPs could encapsulate DNA *via* electrostatic interactions and form S-NPs/DNA nanosystems [148]. Next, the researchers labeled DNA with green fluorescent agent YOYO-1, and incubated HeLa cells with S-NPs/YOYO-1-DNA for 4 h to evaluate the delivery and releasing capability of the system. The results showed that without the light exposure, the red signals from S-NPs largely overlaid with the green signals from YOYO-1-DNA, demonstrating that intracellular S-NPs colocalized with DNA in lysosomes. After light irradiation, the red and green fluorescence signals gradually separated, and the fluorescence colocalization ratios of S-NPs and YOYO-1-DNA decreased significantly, demonstrating a light-induced DNA release. To further trace the process of DNA uptake into the nuclei, HeLa cells were incubated in normal medium for another 4 h and the nuclei were labeled by DRAQ5. It is found that the treatment of S-NPs/YOYO-1-DNA together with light exposure resulted in successful intranuclear transportation of DNA, while S-NPs nanovectors were observed to be dispersed throughout the cytoplasm. In conclusion, certain AIE molecules are potent photosensitizers and can therefore act as "on/off switches" for facilitating and monitoring cellular fates of light-responsive NDDSs.

3.2.3. Redox-responsive NDDSs

Redox-response NDDSs mainly depend on the glutathione (GSH) concentration gradient, which varies from 2-10 μM outside the cell to 2–10 mM in the cellular milieus [128,129]. As one of the common tactics to achieve intracellular redox response, disulfide linkages stay stable when the concentration of GSH is relatively low, but are cleaved rapidly in GSH-rich environments. This feature of disulfide bridges has been employed in the design of various redox-responsive NDDSs for controllable drug release [149–151]. To better monitor the *in vitro* fate of such NDDSs, Hu et al. developed AIE-based DOX-loaded redox-controllable micelles [152]. In this work, the disulfide bonds were employed as the junction between polymer matrix and TPE molecules. The resulting AIE-based vector was used to encapsulate DOX through self-assembly, and finally formed spherical micelles with the diameter of ~123 nm. Once the high concentration of GSH induced the damage of disulfide bonds, the micelle structures broke up, triggering the release of DOX into the cytosol. Next, the research team analyzed the cellular behaviors of these systems in 4T1 cells. After treatment with micelles for 1 h, red fluorescence signals of DOX and blue signals from TPE could be clearly observed in the cytosol. As the co-culture time was prolonged to 3 and 5 h, the intensity of the two signals increased sharply, suggesting the continuous uptake micelles into the cells. After incubation for 7 h, a portion of DOX appeared in the nucleus, whereas the TPE fluorescence was observed throughout the cytoplasm. Thus, with the assistance of AIE agents, researchers are capable of visualizing efficient delivery of drugs carried by NDDSs in response to a change in intracellular GSH concentration.

In conclusion, AIE molecules can be flexibly introduced into NDDSs to utilize their excellent fluorescent properties and capabilities, and thus researchers enable to trace the processes of NDDS endocytosis, breakdown, redistribution, transportation and exocytosis. With the help of AIE-based systems, detailed *in vitro* observations of self-indicating NDDSs have been obtained, and exquisite cellular control of stimuli-responsive NDDSs has been visualized. Further efforts on the exploration of AIE-guided cellular investigation would be required for the design of tailored NDDSs.

4. *In vivo* fate of NDDSs imaged using AIE fluorophores

So far, the AIE-enabled imaging of NDDSs has been mostly amenable to small-scale samples, and has been typically applied to intracellular observations. *In vivo* imaging is however equally important and highly sought-after, as the complex interplay of NDDSs and the living body correlates with therapeutic effect as well as adverse reactions to these systems, especially in repeated exposure to NDDSs [81,153]. In this section, we review the recent advances in long-term observations of therapeutics and their carriers. Moreover, we also focus on *in vivo* studying of the diagnostic properties of AIE-based NDDSs. With the help of AIE agents, it is possible to get thorough insights into the *in vivo* journey of NDDSs to facilitate the development of therapeutic and diagnostic applications of these systems.

4.1. AIE-based NDDSs for long-term tracking of therapeutics

In clinical practice, there is a continuous dilemma of administering higher drug doses that could bring out better therapeutic effects but are accompanied by stronger adverse reactions, especially for systemic administration. Thus, monitoring *in vivo* drug release and distribution to evaluate therapeutic efficacy and safety is highly desirable. Notably, numerous reports have existed about NDDSs that enable the self-indication of dynamic drug behavior in tissues and organs [154–157]. One of practicable tactics is to apply AIE agents to *in vivo* research of NDDSs. Apart from superb photostability, excellent biocompatibility and high sensitivity, AIE fluorophores can provide high-resolution and long-term tracking, which makes them attractive candidates for living body imaging.

DOX has been one of the most ubiquitously used chemotherapeutic agents in clinical oncotherapy, especially for inoperable breast cancer [158,159]. Since the success of Doxil®, there has been an ongoing interest in the investigation of DOX-based NDDSs [7]. However, the grand challenge on long-term visualization of *in vivo* delivery and degradation of such systems still remains. In an attempt to overcome this obstacle, the group of Loh prepared a DOX-loaded thermogel with AIE characteristics [160]. As shown in Fig. 8, they synthesized a novel thermosensitive nanostructure on the basis of TPE, PEG and poly(propylene glycol) agents. In solution, the unique nanostructure enabled to transition from dispersive micelles into closely-packed gel aggregates at 15–45 °C. The unique micelle-gel transformation made it possible to easily encapsulate DOX to fabricate novel sustained-release thermogels. Furthermore, the micelle-gel transition further restricted intramolecular rotation of TPE molecules so that the thermogel featured exceptionally strong fluorescence emission, useful for better self-indicating. Importantly, fluorescence intensity of the thermogel exhibited a sharp increase with decreasing DOX loading concentrations. Therefore, the thermogel has great potential to reflect *in vivo* DOX release behaviors. Using mice with HepG2 tumors, the research team compared *in vivo* drug release of the thermogel NDDS and free DOX drug. In mice which were intratumorally injected with saline DOX, red fluorescence DOX signals appeared as a rapid diffusion into the whole tumor after 3 h. After 24 h, no obvious DOX signals were observed, suggesting that little or no effective DOX remained in the tumor locations. Hence, free DOX underwent rapid diffusion and metabolism *in vivo*. On the contrary, the thermogel DOX exhibited a sustained release, such that strong DOX signals could still be observed even after 14 days. It is also noteworthy that after 18 days, the fluorescence emission from the TPE carriers reduced sharply, which was attributed to the erosion of the thermogel matrix. Therefore, by virtue of AIE fluorophores, researchers could trace the release of drugs and the degradation of their carriers over a long period. These long-term observations would facilitate *in vivo* PK investigations of novel NDDSs to further improve formulation of these agents and their adverse reaction surveillance.

AIE-based NDDSs have also been applied in the detection of *in vivo* distribution of photosensitizers in photodynamic therapy (PDT).

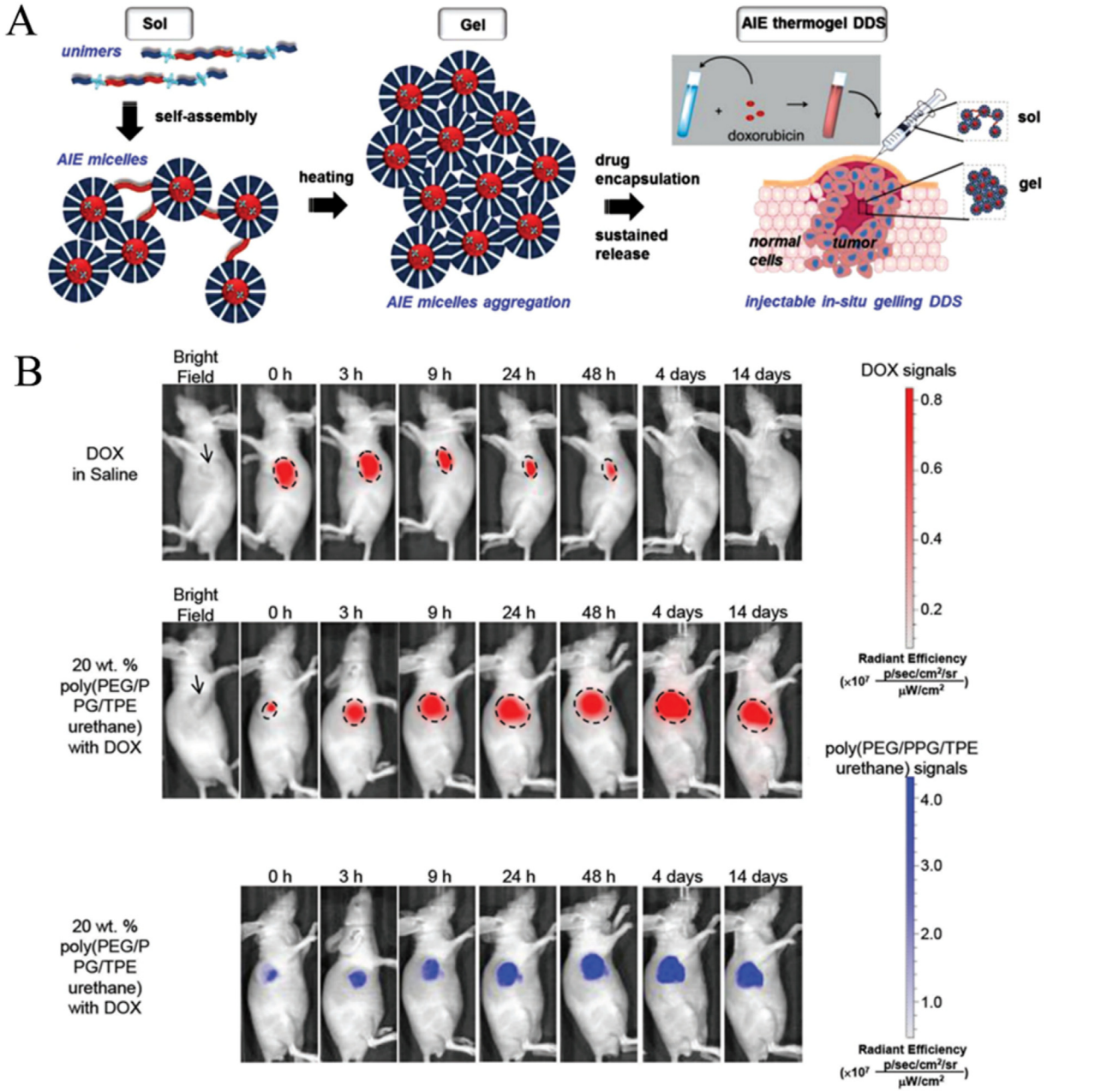

Fig. 8. Long-term visualization of *in vivo* drug release of AIE-based thermogels. (A) AIE-based thermogels were prepared by micelle-gel transition under specific temperatures and encapsulation of DOX. After intratumoral injection, these agents were traceable *in vivo* in mice. (B) Mice bearing HepG2 tumors were treated with free DOX or DOX encapsulated in AIE-containing thermogel NDDSs. The sustained drug release of thermogel could be observed by long-term fluorescence imaging of AIE luminogens. Adapted with permission from [160]. Copyright 2016 John Wiley and Sons.

Under specific irradiation exposure, photosensitizers could trigger the rapid generation of ROS, potentially resulting in severe cellular damage and even cell death [161]. Over the past century, PDT has become a potent strategy for dermatologic treatment, antimicrobial therapy as well as cancer intervention in the clinic [162,163]. Considering high ROS production efficiency and effective fluorescence monitoring of AIE molecules, researchers have been able to employ AIE-based NDDSs for both PDT and *in vivo* tracing. For instance, Li et al. synthesized 40-nm nanodots, termed T-TTD, containing red emissive AIE agents [164]. To analyze the *in vivo* distribution of T-TTD nanodots in mice bearing human cholangiocarcinoma QBC939 tumors, the researchers compared the fluorescence intensity measured in main organs at 12 h post-injection. The results confirmed that T-TTD nanodots concentrated in mice liver and intestine. Meanwhile, strong fluorescence signals also appeared around the tumor sites, revealing that T-TTD nanodots displayed a tumor-selective accumulation. Furthermore, taking advantage of long-term photostability of AIE agents, the research team could track the diffusion of nanodots toward tumors. In the first 2 h after injection, T-TTD dots showed a wide dispersion throughout the body. Then, they appeared to accumulate preferentially in tumor locations as the emissions from tumors showed a dramatic upsurge. Though the whole fluorescence emission underwent a gradual decline after 24 h post-injection, its accumulative distribution in tumor vicinity could still be clearly observed. Even after 48 h post-injection, emission from tumor sites remained strong. Thus, T-TTD nanodots could exhibit a long-term tumor targeting in mice.

In conclusion, AIE fluorophores could assist in unraveling dynamic and long-term interplay between therapeutics and the living body, although few reports of *in vivo* fate of pharmaceutical agents in AIE-based NDDSs are available thus far. Determining how specific organs/

tissues interact with NDDSs would be the key to the development of tailored NDDSs with better *in vivo* therapeutic responses. Therefore, future efforts should be taken in the body-level description of the behavior of NDDSs comprising diverse AIE fluorophores.

4.2. AIE-based NDDSs for multi-modal monitoring of diagnostics

Aside from therapeutic substances, diagnostic materials such as contrast agents also require the elucidation of their *in vivo* fate. In the past few decades, several research groups reported successful multi-modal analysis with the combination of AIE-based fluorophores and other modality agents [108,110]. Thus, chances are that the complementary effects of diverse modalities would offer multi-dimensional observations on the interplay of diagnostics and biosystems to improve the early-stage disease diagnosis.

Using X-rays to scan living samples, deep-penetration and high-resolution imaging of biosystems can be achieved with CT. Since its conception in the 1970s, CT imaging has been progressively employed in clinical diagnosis, offering three-dimensional views of specific body sites [90]. However, the lack of sensitivity has been considered as the Achilles' heel of CT imaging. In addition, CT contrast agents such as gold nanoparticles (Au NPs) are prone to induce strong fluorophore quenching effects when introduced together with conventional fluorescent molecules, [165]. Hence, it is rather difficult to apply a combination of fluorescence/CT imaging. Fortunately, with the advantage of high sensitivity and unique fluorescence emissions, AIE-based imaging can be used complementary to CT imaging. As shown in Fig. 9, Zhang et al. employed Au NPs as CT contrast agents and bis(4-(N-(2-naphthyl) phenylamino)phenyl)-fumaronitrile (NPAPF) as AIE fluorophores to generate M-NPAPF-Au NDDSs [166]. They confirmed that M-NPAPF-Au showed no obvious cytotoxicity in CT26, HepG2 and L02 cells. Measuring the Hounsfield units, they also verified that M-NPAPF-Au could serve as a superior tumor-targeting CT imaging agent in CT62 tumor-bearing mice. Next, to investigate the *in vivo* behaviors of M-NPAPF-Au, they compared fluorescence images of the mice bodies to those of separated tissues and organs at different time points. The results showed that at 24 h after injection, strong fluorescence signals appeared in the tumor sites, showing that M-NPAPF-Au could successfully accumulate in tumors due to the EPR effect. Furthermore, because of the uptake capacity of RES, M-NAPAPF-Au also exhibited a dense distribution in the liver and spleen. Therefore, M-NAPAPF-Au can be exploited as a potent dual-mode fluorescence/micro CT diagnostics delivery system. As the standard CT scans usually require large doses of contrast agents as well as exposure to radiation, the synergistic action of CT technology and fluorescent agents could also reduce the risks to patients.

As mentioned above, the combination of AIE-based fluorescence imaging and other modalities could provide new opportunities for monitoring *in vivo* biodistribution of diagnostics and tracing their elimination from a living body. With a better understanding of how diagnostics interact with biosystems, designer NDDSs can be produced for multi-stage disease diagnosis with high accuracy, high sensitivity and low toxicity.

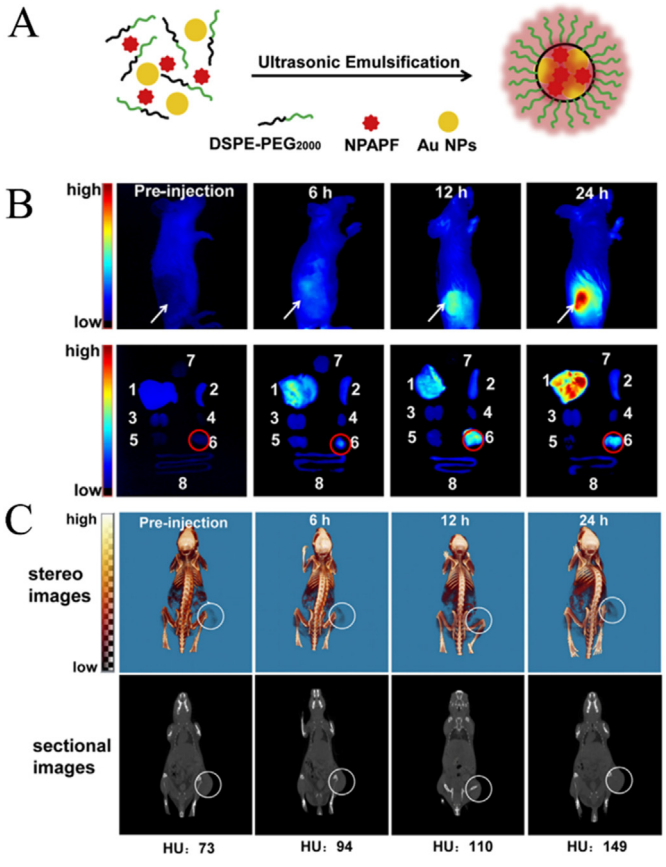

Fig. 9. Combined fluorescence/CT imaging of the *in vivo* distribution of M-NPAPF-Au nanostructures. (A) The dual-modality NDDSs were constructed using NPAPF as AIE fluorophores and Au NPs as CT contrast agents. (B) Fluorescence images and (C) CT images of mice bearing CT26 tumors and their tissues and organs after injection of M-NPAPF-Au. Tumor locations in mice were denoted with white arrows and the dissected tumor tissues were indicated by red and white circles. High signal intensity in tumor sites indicated the tumor-preferential accumulation of M-NPAPF-Au. Adapted with permission from [166].

5. Conclusion and perspectives

With unique physicochemical and biological properties, NDDSs have attracted much attention in pharmaceutical and biological research. The efficacy of these nanostructures mainly depends on their behaviors in living environments. Therefore, it is of great importance to visualize the biological itinerary of NDDSs with the assistance of imaging tools. In this review, we highlight the investigations of NDDSs' biological fate by the application of AIE fluorophores. As for the *in vitro* fate, we focus on the AIE-guided tracing of self-indicating and stimuli-responsive NDDSs. High-resolution, high-sensitivity and real-time imaging of AIE agents enable researchers to get deeper insights into the processes of intracellular activation, breakdown and distribution of NDDSs and their carriers and cargos. Aside from cellular behaviors, we also review *in vivo* distribution and degradation of NDDSs which are loaded with therapeutic or diagnostic agents. Capable of long-term and multi-modal tracking, AIE luminogens can be promising candidates in the tracing of NDDSs' *in vivo* fate.

Despite the described advances, there still maintain rigorous challenges. Firstly, more efforts should be taken to elucidate the potential influence of AIE modification on NDDSs. It is reported that several AIE molecules enable to induce ROS generation in biological environments [101,146,167]. Thus, their bioactivity may affect therapeutic actions of NDDSs. In previous studies, simple quantitative parameters (half maximal inhibitory concentration, minimum inhibitory concentration, cell viability, *etc.*), have been used to evaluate whether AIE molecules would affect final therapeutic actions of NDDSs [103,37]. Nonetheless, little is known whether the incorporation of AIE molecules into NDDSs affects the pharmaceutical properties of the cargos, such as conformation of chemical structures, peptide folding and nucleotide stability. To realize objective and reliable visualization about how NDDSs interact with biosystems, researchers should exclude negative influences of AIE agents on NDDSs. Secondly, it is necessary to investigate the stability of AIE-based NDDSs in bioimaging. Unstable connections between AIE molecules and NDDSs may induce unexpected disassembly of AIE agents. Once the released AIE agents form aggregates, false fluorescent emissions would cause unreliability. Thus, researchers should discriminate fluorescent signals of integral NDDSs from released AIE agents. More strategies are needed to eliminate false positive signals. More

importantly, the biosafety of AIE fluorophores, such as long-term toxicity, genetic toxicity and immunogenicity, also remains to be assessed in detail. Due to the complexity and disparity of experimental designs (cell/animal models, growth conditions, administration routes, monitoring duration, *etc.*), it is difficult to carry out rational and systematic comparisons between experiments. Thus, a clear emphasis lies in building up benchmarking guidelines on AIE-guided evaluation of NDDS biological behaviors. Such agreement could strongly accelerate the clinical translation of NDDSs. Alongside these concerns, future work on visualizing the biological fate of NDDSs with AIE agents should be focused on the following three aspects. The first is to propose AIE-based analysis of different NDDS cellular behaviors in different cells, especially in monocytes and Kupffer cells which are related to the clearance and excretion of NDDSs. Secondly, as for the *in vivo* fate, it is still unclear how NDDSs cross physiological and pathological barriers, such as blood brain barrier, placental barrier and tumor interstitium. Equally important is the exploration of the interaction between NDDSs and the immune system, as the breakup of immune balance could cause severe adverse reactions in the whole body. Moreover, to realize better *in vivo* imaging, more efforts should be taken into the exploitation of AIE fluorophores with near-infrared emissions. Overall, it has been shown that AIE fluorophores offer flexible controllability, advantageous biocompatibility and superb imaging quality. These unique properties make them promising candidates for visualizing both *in vitro* and *in vivo* fate of NDDSs. We believe that the in-depth understanding of NDDS biological fates will facilitate the generation of effective and safe strategies for clinical treatment and diagnosis.

Acknowledgements

This work was supported by the National Natural Science Foundation key project (31630027 and 31430031), National Natural Science Foundation project (31600808) and NSFC-DFG project (31761133013). The authors also appreciate the support by the "Strategic Priority Research Program" of the Chinese Academy of Sciences, Grant No. XDA09030301. They also thank Dr. Maria Matveenko (*Life Science Editors*) for language editing.

References

[1] C. Chiappini, E. De Rosa, J.O. Martinez, X. Liu, J. Steele, M.M. Stevens, E. Tasciotti, Biodegradable silicon nanoneedles delivering nucleic acids intracellularly induce localized in vivo neovascularization, Nat. Mater. 14 (2015) 532–539.
[2] X. Liu, X. Jin, P.X. Ma, Nanofibrous hollow microspheres self-assembled from star-shaped polymers as injectable cell carriers for knee repair, Nat. Mater. 10 (2011) 398–406.
[3] X. Xue, J.-Y. Yang, Y. He, L.-R. Wang, P. Liu, L.-S. Yu, G.-H. Bi, M.-M. Zhu, Y.-Y. Liu, R.-W. Xiang, X.-T. Yang, X.-Y. Fan, X.-M. Wang, J. Qi, H.-J. Zhang, T. Wei, W. Cui, G.-L. Ge, Z.-X. Xi, C.-F. Wu, X.-J. Liang, Aggregated single-walled carbon nanotubes attenuate the behavioural and neurochemical effects of methamphetamine in mice, Nat. Nanotechnol. 11 (2016) 613–620.
[4] T. Wei, C. Chen, J. Liu, C. Liu, P. Posocco, X. Liu, Q. Cheng, S. Huo, Z. Liang, M. Fermeglia, S. Pricl, X.-J. Liang, P. Rocchi, L. Peng, Anticancer drug nanomicelles formed by self-assembling amphiphilic dendrimer to combat cancer drug resistance, Proc. Natl. Acad. Sci. U. S. A. 112 (2015) 2978–2983.
[5] V. Narasimhan, R.H. Siddique, J.O. Lee, S. Kumar, B. Ndjamen, J. Du, N. Hong, D. Sretavan, H. Choo, Multifunctional biophotonic nanostructures inspired by the longtail glasswing butterfly for medical devices, Nat. Nanotechnol. 13 (2018) 512–519.
[6] B. Zhang, B.A. Pinsky, J.S. Ananta, S. Zhao, S. Arulkumar, H. Wan, M.K. Sahoo, J. Abeynayake, J.J. Waggoner, C. Hopes, M. Tang, H. Dai, Diagnosis of Zika virus infection on a nanotechnology platform, Nat. Med. 23 (2017) 548–550.
[7] Y. Barenholz, Doxil®—the first FDA-approved nano-drug: Lessons learned, J. Control. Release 160 (2012) 117–134.
[8] M.J. Hawkins, P. Soon-Shiong, N. Desai, Protein nanoparticles as drug carriers in clinical medicine, Adv. Drug Deliv. Rev. 60 (2008) 876–885.
[9] Drugs@FDA, FDA Approved Drug Products NDA210922, https://www.accessdata.fda.gov/scripts/cder/daf/index.cfm?event=overview.process&varApplNo=210922 2018, Accessed date: 8 December 2018.
[10] W. Chen, J. Ouyang, H. Liu, M. Chen, K. Zeng, J. Sheng, Z. Liu, Y. Han, L. Wang, J. Li, L. Deng, Y.-N. Liu, S. Guo, Black phosphorus nanosheet-based drug delivery system for synergistic photodynamic/photothermal/chemotherapy of cancer, Adv. Mater. 29 (2016) 1603864–1603870.
[11] F. Peng, Y. Su, X. Wei, Y. Lu, Y. Zhou, Y. Zhong, S.-T. Lee, Y. He, Silicon-nanowire-based nanocarriers with ultrahigh drug-loading capacity for in vitro and in vivo cancer therapy, Angew. Chem. Int. Ed. 52 (2012) 1457–1461.
[12] Z. Gu, Q. Wang, Y. Shi, Y. Huang, J. Zhang, X. Zhang, G. Lin, Nanotechnology-mediated immunochemotherapy combined with docetaxel and PD-L1 antibody increase therapeutic effects and decrease systemic toxicity, J. Control. Release 286 (2018) 369–380.
[13] Y. Han, B. Ding, Z. Zhao, H. Zhang, B. Sun, Y. Zhao, L. Jiang, J. Zhou, Y. Ding, Immune lipoprotein nanostructures inspired relay drug delivery for amplifying antitumor efficiency, Biomaterials 185 (2018) 205–218.
[14] B. Mao, C. Liu, W. Zheng, X. Li, R. Ge, H. Shen, X. Guo, Q. Lian, X. Shen, C. Li, Cyclic cRGDfk peptide and Chlorin e6 functionalized silk fibroin nanoparticles for targeted drug delivery and photodynamic therapy, Biomaterials 161 (2018) 306–320.
[15] N. Bertrand, J. Wu, X. Xu, N. Kamaly, O.C. Farokhzad, Cancer nanotechnology: the impact of passive and active targeting in the era of modern cancer biology, Adv. Drug Deliv. Rev. 66 (2014) 2–25.
[16] V.P. Torchilin, Multifunctional, stimuli-sensitive nanoparticulate systems for drug delivery, Nat. Rev. Drug Discov. 13 (2014) 813–827.
[17] X. Tan, S. Luo, L. Long, Y. Wang, D. Wang, S. Fang, Q. Ouyang, Y. Su, T. Cheng, C. Shi, Structure-guided design and synthesis of a mitochondria-targeting near-infrared fluorophore with multimodal therapeutic activities, Adv. Mater. 29 (2017) 1704196–1704204.
[18] J. Liu, P. Wang, X. Zhang, L. Wang, D. Wang, Z. Gu, J. Tang, M. Guo, M. Cao, H. Zhou, Y. Liu, C. Chen, Rapid degradation and high renal clearance of Cu3BiS3 nanodots for efficient cancer diagnosis and photothermal therapy in vivo, ACS Nano 10 (2016) 4587–4598.
[19] C. Zeng, W. Shang, X. Liang, X. Liang, Q. Chen, C. Chi, Y. Du, C. Fang, J. Tian, Cancer diagnosis and imaging-guided photothermal therapy using a dual-modality nanoparticle, ACS Appl. Mater. Interfaces 8 (2016) 29232–29241.
[20] G. Griffiths, B. Nyström, S.B. Sable, G.K. Khuller, Nanobead-based interventions for the treatment and prevention of tuberculosis, Nat. Rev. Microbiol. 8 (2010) 827–834.
[21] Y. Chao, Y. Liang, G. Fang, H. He, Q. Yao, H. Xu, Y. Chen, X. Tang, Biodegradable polymersomes as nanocarriers for doxorubicin hydrochloride: enhanced cytotoxicity in MCF-7/ADR cells and prolonged blood circulation, Pharm. Res. 34 (2017) 610–618.
[22] H.-X. Wang, Z.-Q. Zuo, J.-Z. Du, Y.-C. Wang, R. Sun, Z.-T. Cao, X.-D. Ye, J.-L. Wang, K.W. Leong, J. Wang, Surface charge critically affects tumor penetration and therapeutic efficacy of cancer nanomedicines, Nano Today 11 (2016) 133–144.
[23] A. Dickherber, S.A. Morris, P. Grodzinski, NCI investment in nanotechnology: achievements and challenges for the future, Wiley Interdiscip. Rev. Nanomed. Nanobiotechnol. 7 (2015) 251–265.
[24] M.A. Eaton, L. Levy, O.M. Fontaine, Delivering nanomedicines to patients: a practical guide, Nanomedicine 11 (2015) 983–992.
[25] C.W. Noorlander, M.W. Kooi, A.G. Oomen, M.V.D.Z. Park, R.J. Vandebriel, R.E. Geertsma, Horizon scan of nanomedicinal products, Nanomedicine 10 (2015) 1599–1608.
[26] B. Vandeginste, R. Essers, T. Bosman, J. Reijnen, G. Kateman, Three-component curve resolution in liquid chromatography with multiwavelength diode array detection, Anal. Chem. 57 (1985) 971–985.
[27] B.M. Simonet, A. Rios, M. Valcárcel, Enhancing sensitivity in capillary electrophoresis, TrAC Trends Anal. Chem. 22 (2003) 605–614.
[28] J. Wu, Z. Fu, F. Yan, H. Ju, Biomedical and clinical applications of immunoassays and immunosensors for tumor markers, TrAC, Trends Anal. Chem. 26 (2007) 679–688.
[29] B. Wan, Y. Dai, D. Liu, J. Qi, X. Dong, W. Zhao, W. Wu, Y. Lu, Intraocular fate of polycaprolactone nanoparticles administered via intravitreal and various periocular routes: bioimaging of integral nanoparticles using environment-sensitive fluorophores, J. Biomed. Nanotechnol. 13 (2017) 960–972.
[30] P. Ning, W. Wang, M. Chen, Y. Feng, X. Meng, Recent advances in mitochondria- and lysosomes-targeted small-molecule two-photon fluorescent probes, Chin. Chem. Lett. 28 (2017) 1943–1951.
[31] J. Luo, Z. Xie, J.W.Y. Lam, L. Cheng, H. Chen, C. Qiu, H.S. Kwok, X. Zhan, Y. Liu, D. Zhu, B.Z. Tang, Aggregation-induced emission of 1-methyl-1,2,3,4,5-pentaphenylsilole, Chem. Commun. (2001) 1740–1741.
[32] M.S.T. Gonçalves, Fluorescent labeling of biomolecules with organic probes, Chem. Rev. 109 (2009) 190–212.
[33] M. Noh, T. Kim, H. Lee, C.-K. Kim, S.-W. Joo, K. Lee, Fluorescence quenching caused by aggregation of water-soluble CdSe quantum dots, Colloids Surf. Physicochem. Eng. Asp. 359 (2010) 39–44.
[34] J. Mei, N.L.C. Leung, R.T.K. Kwok, J.W.Y. Lam, B.Z. Tang, Aggregation-induced emission: together we shine, united we soar! Chem. Rev. 115 (2015) 11718–11940.
[35] S. Chen, H. Wang, Y. Hong, B.Z. Tang, Fabrication of fluorescent nanoparticles based on AIE luminogens (AIE dots) and their applications in bioimaging, Mater. Horiz. 3 (2016) 283–293.
[36] H. Shi, R.T.K. Kwok, J. Liu, B. Xing, B.Z. Tang, B. Liu, Real-time monitoring of cell apoptosis and drug screening using fluorescent light-up probe with aggregation-induced emission characteristics, J. Am. Chem. Soc. 134 (2012) 17972–17981.
[37] E. Zhao, Y. Chen, S. Chen, H. Deng, C. Gui, W.T. Leung Chris, Y. Hong, W.Y. Lam Jacky, Z. Tang Ben, A luminogen with aggregation-induced emission characteristics for wash-free bacterial imaging, high-throughput antibiotics screening and bacterial susceptibility evaluation, Adv. Mater. 27 (2015) 4931–4937.
[38] N.L.C. Leung, N. Xie, W. Yuan, Y. Liu, Q. Wu, Q. Peng, Q. Miao, J.W.Y. Lam, B.Z. Tang, Restriction of intramolecular motions: the general mechanism behind aggregation-induced emission, Chem. Eur. J. 20 (2014) 15349–15353.

[39] J. Mei, Y. Hong, W.Y. Lam Jacky, A. Qin, Y. Tang, Z. Tang Ben, Aggregation-induced emission: the whole is more brilliant than the parts, Adv. Mater. 26 (2014) 5429–5479.
[40] J. Luo, K. Song, F.L. Gu, Q. Miao, Switching of non-helical overcrowded tetrabenzoheptafulvalene derivatives, Chem. Sci. 2 (2011) 2029–2034.
[41] Z. He, C. Ke, B.Z. Tang, Journey of aggregation-induced emission research, ACS Omega 3 (2018) 3267–3277.
[42] S. Choi, J. Bouffard, Y. Kim, Aggregation-induced emission enhancement of a meso-trifluoromethyl BODIPY via J-aggregation, Chem. Sci. 5 (2014) 751–755.
[43] P. Chen, R. Lu, P. Xue, T. Xu, G. Chen, Y. Zhao, Emission enhancement and chromism in a salen-based gel system, Langmuir 25 (2009) 8395–8399.
[44] P. Zhang, H. Wang, H. Liu, M. Li, Fluorescence-enhanced organogels and mesomorphic superstructure based on hydrazine derivatives, Langmuir 26 (2010) 10183–10190.
[45] B.-K. An, S.-K. Kwon, S.-D. Jung, S.Y. Park, Enhanced emission and its switching in fluorescent organic nanoparticles, J. Am. Chem. Soc. 124 (2002) 14410–14415.
[46] T. He, N. Niu, Z. Chen, S. Li, S. Liu, J. Li, Novel quercetin aggregation-induced emission luminogen (AIEgen) with excited-state intramolecular proton transfer for in vivo bioimaging, Adv. Funct. Mater. 28 (2018) 1706196–1706203.
[47] S. Li, L. He, F. Xiong, Y. Li, G. Yang, Enhanced fluorescent emission of organic nanoparticles of an intramolecular proton transfer compound and spontaneous formation of one-dimensional nanostructures, J. Phys. Chem. B 108 (2004) 10887–10892.
[48] Q. Chen, C. Jia, Y. Zhang, W. Du, Y. Wang, Y. Huang, Q. Yang, Q. Zhang, A novel fluorophore based on the coupling of AIE and ESIPT mechanisms and its application in biothiol imaging, J. Mater. Chem. B 5 (2017) 7736–7742.
[49] Y. Dong, J.W.Y. Lam, A. Qin, J. Liu, Z. Li, B.Z. Tang, J. Sun, H.S. Kwok, Aggregation-induced emissions of tetraphenylethene derivatives and their utilities as chemical vapor sensors and in organic light-emitting diodes, Appl. Phys. Lett. 91 (2007), 011111.
[50] B.-K. An, J. Gierschner, S.Y. Park, π-Conjugated cyanostilbene derivatives: a unique self-assembly motif for molecular nanostructures with enhanced emission and transport, Acc. Chem. Res. 45 (2012) 544–554.
[51] W.Z. Yuan, P. Lu, S. Chen, J.W.Y. Lam, Z. Wang, Y. Liu, H.S. Kwok, Y. Ma, B.Z. Tang, Changing the behavior of chromophores from aggregation-caused quenching to aggregation-induced emission: development of highly efficient light emitters in the solid state, Adv. Mater. 22 (2010) 2159–2163.
[52] Z. Zhao, Z. Wang, P. Lu, C.Y.K. Chan, D. Liu, J.W.Y. Lam, H.H.Y. Sung, I.D. Williams, Y. Ma, B.Z. Tang, Structural modulation of solid-state emission of 2,5-Bis (trialkylsilylethynyl)-3,4-diphenylsiloles, Angew. Chem. Int. Ed. 48 (2009) 7608–7611.
[53] J. Zhou, B. He, B. Chen, P. Lu, H.H.Y. Sung, I.D. Williams, A. Qin, H. Qiu, Z. Zhao, B.Z. Tang, Deep blue fluorescent 2,5-bis(phenylsilyl)-substituted 3,4-diphenylsiloles: Synthesis, structure and aggregation-induced emission, Dyes Pigments 99 (2013) 520–525.
[54] L. Chen, Y. Jiang, H. Nie, P. Lu, H.H.Y. Sung, I.D. Williams, H.S. Kwok, F. Huang, A. Qin, Z. Zhao, B.Z. Tang, Creation of bifunctional materials: improve electron-transporting ability of light emitters based on AIE-Active 2,3,4,5-tetraphenylsiloles, Adv. Funct. Mater. 24 (2014) 3621–3630.
[55] M.Z. Chen, N.S. Moily, J.L. Bridgford, R.J. Wood, M. Radwan, T.A. Smith, Z. Song, B.Z. Tang, L. Tilley, X. Xu, G.E. Reid, M.A. Pouladi, Y. Hong, D.M. Hatters, A thiol probe for measuring unfolded protein load and proteostasis in cells, Nat. Commun. 8 (2017) 474–484.
[56] T. Zhang, W. Guo, C. Zhang, J. Yu, J. Xu, S. Li, J.-H. Tian, P.C. Wang, J.-F. Xing, X.-J. Liang, Transferrin-dressed virus-like ternary nanoparticles with aggregation-induced emission for targeted delivery and rapid cytosolic release of siRNA, ACS Appl. Mater. Interfaces 9 (2017) 16006–16014.
[57] B. Gu, W. Wu, G. Xu, G. Feng, F. Yin, J. Chong Peter Han, J. Qu, K.-T. Yong, B. Liu, Precise two-photon photodynamic therapy using an efficient photosensitizer with aggregation-induced emission characteristics, Adv. Mater. 29 (2017) 1701076–1701082.
[58] A. Nicol, R.T.K. Kwok, C. Chen, W. Zhao, M. Chen, J. Qu, B.Z. Tang, Ultrafast delivery of aggregation-induced emission nanoparticles and pure organic phosphorescent nanocrystals by saponin encapsulation, J. Am. Chem. Soc. 139 (2017) 14792–14799.
[59] Q. Xia, Z. Chen, Z. Yu, L. Wang, J. Qu, R. Liu, Aggregation-induced emission-active near-infrared fluorescent organic nanoparticles for noninvasive long-term monitoring of tumor growth, ACS Appl. Mater. Interfaces 10 (2018) 17081–17088.
[60] Y. Yuan, C.-J. Zhang, M. Gao, R. Zhang, Z. Tang Ben, B. Liu, Specific light-up bioprobe with aggregation-induced emission and activatable photoactivity for the targeted and image-guided photodynamic ablation of cancer cells, Angew. Chem. Int. Ed. 54 (2014) 1780–1786.
[61] C. Zhang, S. Jin, K. Yang, X. Xue, Z. Li, Y. Jiang, W.-Q. Chen, L. Dai, G. Zou, X.-J. Liang, Cell membrane tracker based on restriction of intramolecular rotation, ACS Appl. Mater. Interfaces 6 (2014) 8971–8975.
[62] X. Wang, Y. Yang, Y. Zhuang, P. Gao, F. Yang, H. Shen, H. Guo, D. Wu, Fabrication of pH-responsive nanoparticles with an AIE feature for imaging intracellular drug delivery, Biomacromolecules 17 (2016) 2920–2929.
[63] K. Han, S.-B. Wang, Q. Lei, J.-Y. Zhu, X.-Z. Zhang, Ratiometric biosensor for aggregation-induced emission-guided precise photodynamic therapy, ACS Nano 9 (2015) 10268–10277.
[64] H. Lu, X. Zhao, W. Tian, Q. Wang, J. Shi, Pluronic F127-folic acid encapsulated nanoparticles with aggregation-induced emission characteristics for targeted cellular imaging, RSC Adv. 4 (2014) 18460–18466.
[65] Y. Liu, X. Zhang, M. Zhou, X. Chen, X. Zhang, Surface engineering of organic nanoparticles for highly improved bioimaging, Colloids Surf. B Biointerfaces 159 (2017) 596–604.
[66] J. Qi, C. Sun, A. Zebibula, H. Zhang, T.K. Kwok Ryan, X. Zhao, W. Xi, W.Y. Lam Jacky, J. Qian, Z. Tang Ben, Real-time and high-resolution bioimaging with bright aggregation-induced emission dots in short-wave infrared region, Adv. Mater. 30 (2018) 1706856–1706864.
[67] M. Jiang, X. Gu, J.W.Y. Lam, Y. Zhang, R.T.K. Kwok, K.S. Wong, B.Z. Tang, Two-photon AIE bio-probe with large Stokes shift for specific imaging of lipid droplets, Chem. Sci. 8 (2017) 5440–5446.
[68] D. Ding, R.T.K. Kwok, Y. Yuan, G. Feng, B.Z. Tang, B. Liu, A fluorescent light-up nanoparticle probe with aggregation-induced emission characteristics and tumor-acidity responsiveness for targeted imaging and selective suppression of cancer cells, Mater. Horiz. 2 (2015) 100–105.
[69] H. Shi, J. Liu, J. Geng, B.Z. Tang, B. Liu, Specific detection of integrin αvβ3 by light-up bioprobe with aggregation-induced emission characteristics, J. Am. Chem. Soc. 134 (2012) 9569–9572.
[70] Y. Min, K.C. Roche, S. Tian, M.J. Eblan, K.P. McKinnon, J.M. Caster, S. Chai, L.E. Herring, L. Zhang, T. Zhang, J.M. Desimone, J.E. Tepper, B.G. Vincent, J.S. Serody, A.Z. Wang, Antigen-capturing nanoparticles improve the abscopal effect and cancer immunotherapy, Nat. Nanotechnol. 12 (2017) 877–882.
[71] B.Q. Spring, R. Bryan Sears, L.Z. Zheng, Z. Mai, R. Watanabe, M.E. Sherwood, D.A. Schoenfeld, B.W. Pogue, S.P. Pereira, E. Villa, T. Hasan, A photoactivable multi-inhibitor nanoliposome for tumour control and simultaneous inhibition of treatment escape pathways, Nat. Nanotechnol. 11 (2016) 378–387.
[72] M. Kovarova, S.R. Benhabbour, I. Massud, R.A. Spagnuolo, B. Skinner, C.E. Baker, C. Sykes, K.R. Mollan, A.D.M. Kashuba, J.G. García-Lerma, R.J. Mumper, J.V. Garcia, Ultra-long-acting removable drug delivery system for HIV treatment and prevention, Nat. Commun. 9 (2018) 4156–4166.
[73] G. Yang, L. Xu, Y. Chao, J. Xu, X. Sun, Y. Wu, R. Peng, Z. Liu, Hollow MnO2 as a tumor-microenvironment-responsive biodegradable nano-platform for combination therapy favoring antitumor immune responses, Nat. Commun. 8 (2017) 902–1004.
[74] J. Conde, N. Oliva, Y. Zhang, N. Artzi, Local triple-combination therapy results in tumour regression and prevents recurrence in a colon cancer model, Nat. Mater. 15 (2016) 1128–1140.
[75] J. Guan, Q. Shen, Z. Zhang, Z. Jiang, Y. Yang, M. Lou, J. Qian, W. Lu, C. Zhan, Enhanced immunocompatibility of ligand-targeted liposomes by attenuating natural IgM absorption, Nat. Commun. 9 (2018) 2982–2992.
[76] A. Braunová, L. Kostka, L. Sivák, L. Cuchalová, Z. Hvězdová, R. Laga, S. Filippov, P. Černoch, M. Pechar, O. Janoušková, M. Šírová, T. Etrych, Tumor-targeted micelle-forming block copolymers for overcoming of multidrug resistance, J. Control. Release 245 (2017) 41–51.
[77] M. Li, K.T. Al-Jamal, K. Kostarelos, J. Reineke, Physiologically based pharmacokinetic modeling of nanoparticles, ACS Nano 4 (2010) 6303–6317.
[78] S. Onoue, S. Yamada, H.-K. Chan, Nanodrugs: pharmacokinetics and safety, Int. J. Nanomedicine 9 (2014) 1025–1037.
[79] W.I. Hagens, A.G. Oomen, W.H. de Jong, F.R. Cassee, A.J.A.M. Sips, What do we (need to) know about the kinetic properties of nanoparticles in the body? Regul. Toxicol. Pharmacol. 49 (2007) 217–229.
[80] B.T. Griffin, J. Guo, E. Presas, M.D. Donovan, M.J. Alonso, C.M. O'Driscoll, Pharmacokinetic, pharmacodynamic and biodistribution following oral administration of nanocarriers containing peptide and protein drugs, Adv. Drug Deliv. Rev. 106 (2016) 367–380.
[81] J. Bourquin, A. Milosevic, D. Hauser, R. Lehner, F. Blank, A. Petri-Fink, B. Rothen-Rutishauser, Biodistribution, clearance, and long-term fate of clinically relevant nanomaterials, Adv. Mater. 30 (2018) 1704307–1704337.
[82] L. Tan, B. Ma, Qian Zhao, Lan Zhang, L. Chen, J. Peng, Z. Qian, Toxicity evaluation and anti-tumor study of docetaxel loaded mPEG-polyester micelles for breast cancer therapy, J. Biomed. Nanotechnol. 13 (2017) 393–408.
[83] J. Wang, Q. Liu, L. Yang, X. Xia, R. Zhu, S. Chen, M. Wang, L. Cheng, X. Wu, S. Wang, Curcumin-loaded TPGS/F127/P123 mixed polymeric micelles for cervical cancer therapy: formulation, characterization, and in vitro and in vivo evaluation, J. Biomed. Nanotechnol. 13 (2017) 1631–1646.
[84] A. Woods, A. Patel, D. Spina, Y. Riffo-Vasquez, A. Babin-Morgan, R.T.M. de Rosales, K. Sunassee, S. Clark, H. Collins, K. Bruce, L.A. Dailey, B. Forbes, In vivo biocompatibility, clearance, and biodistribution of albumin vehicles for pulmonary drug delivery, J. Control. Release 210 (2015) 1–9.
[85] L. Tang, X. Yang, Q. Yin, K. Cai, H. Wang, I. Chaudhury, C. Yao, Q. Zhou, M. Kwon, J.A. Hartman, I.T. Dobrucki, L.W. Dobrucki, L.B. Borst, S. Lezmi, W.G. Helferich, A.L. Ferguson, T.M. Fan, J. Cheng, Investigating the optimal size of anticancer nanomedicine, Proc. Natl. Acad. Sci. U. S. A. 111 (2014) 15344–15349.
[86] S. Kunjachan, F. Gremse, B. Theek, P. Koczera, R. Pola, M. Pechar, T. Etrych, K. Ulbrich, G. Storm, F. Kiessling, T. Lammers, Noninvasive optical imaging of nanomedicine biodistribution, ACS Nano 7 (2013) 252–262.
[87] M.A. Miller, S. Gadde, C. Pfirschke, C. Engblom, M.M. Sprachman, R.H. Kohler, K.S. Yang, A.M. Laughney, G. Wojtkiewicz, N. Kamaly, S. Bhonagiri, M.J. Pittet, O.C. Farokhzad, R. Weissleder, Predicting therapeutic nanomedicine efficacy using a companion magnetic resonance imaging nanoparticle, Sci. Transl. Med. 7 (2015) 314ra183, https://doi.org/10.1126/scitranslmed.aac6522.
[88] S.S. Gambhir, Molecular imaging of cancer with positron emission tomography, Nat. Rev. Cancer 2 (2002) 683–693.
[89] R.J. Hicks, M.S. Hofman, Is there still a role for SPECT–CT in oncology in the PET–CT era? Nat. Rev. Clin. Oncol. 9 (2012) 712–720.
[90] D.J. Brenner, E.J. Hall, Computed tomography—an increasing source of radiation exposure, N. Engl. J. Med. 357 (2007) 2277–2284.
[91] R. Huzjan, E. Sala, H. Hricak, Magnetic resonance imaging and magnetic resonance spectroscopic imaging of prostate cancer, Nat. Clin. Pract. Urol. 2 (2005) 434–442.
[92] J. Lippincott-Schwartz, G.H. Patterson, Development and use of fluorescent protein markers in living cells, Science 300 (2003) 87–91.

[93] X. Liu, L. Yang, Q. Long, D. Weaver, G. Hajnóczky, Choosing proper fluorescent dyes, proteins, and imaging techniques to study mitochondrial dynamics in mammalian cells, Biophys. Rep. 3 (2017) 64–72.
[94] N. Boute, R. Jockers, T. Issad, The use of resonance energy transfer in high-throughput screening: BRET versus FRET, Trends Pharmacol. Sci. 23 (2002) 351–354.
[95] E.W. Miller, J.Y. Lin, E.P. Frady, P.A. Steinbach, W.B. Kristan, R.Y. Tsien, Optically monitoring voltage in neurons by photo-induced electron transfer through molecular wires, Proc. Natl. Acad. Sci. 109 (2012) 2114–2119.
[96] Z. Zhu, J. Qian, X. Zhao, W. Qin, R. Hu, H. Zhang, D. Li, Z. Xu, B.Z. Tang, S. He, Stable and size-tunable aggregation-induced emission nanoparticles encapsulated with nanographene oxide and applications in three-photon fluorescence bioimaging, ACS Nano 10 (2016) 588–597.
[97] Y. Chen, H. Han, H. Tong, T. Chen, H. Wang, J. Ji, Q. Jin, Zwitterionic phosphorylcholine–TPE conjugate for pH-responsive drug delivery and AIE active imaging, ACS Appl. Mater. Interfaces 8 (2016) 21185–21192.
[98] Y. Song, L. Zong, L. Zhang, Z. Li, To form AIE product with the target analyte: a new strategy for excellent fluorescent probes, and convenient detection of hydrazine in seconds with test strips, Sci. China Chem. 60 (2017) 1596–1601.
[99] X. Zhang, K. Wang, M. Liu, X. Zhang, L. Tao, Y. Chen, Y. Wei, Polymeric AIE-based nanoprobes for biomedical applications: recent advances and perspectives, Nanoscale 7 (2015) 11486–11508.
[100] L. Wang, Q. Xia, M. Hou, C. Yan, Y. Xu, J. Qu, R. Liu, A photostable cationic fluorophore for long-term bioimaging, J. Mater. Chem. B 5 (2017) 9183–9188.
[101] W. Wu, D. Mao, F. Hu, S. Xu, C. Chen, C.-J. Zhang, X. Cheng, Y. Yuan, D. Ding, D. Kong, B. Liu, A highly efficient and photostable photosensitizer with near-infrared aggregation-induced emission for image-guided photodynamic anticancer therapy, Adv. Mater. 29 (2017) 1700548.
[102] Z. Wang, T.-Y. Yong, J. Wan, Z.-H. Li, H. Zhao, Y. Zhao, L. Gan, X.-L. Yang, H.-B. Xu, C. Zhang, Temperature-sensitive fluorescent organic nanoparticles with aggregation-induced emission for long-term cellular tracing, ACS Appl. Mater. Interfaces 7 (2015) 3420–3425.
[103] X.D. Xue, Y.Y. Zhao, L.R. Dai, X. Zhang, X.H. Hao, C.Q. Zhang, S.D. Huo, J. Liu, C. Liu, A. Kumar, W.Q. Chen, G.Z. Zou, X.J. Liang, Spatiotemporal drug release visualized through a drug delivery system with tunable aggregation-induced emission, Adv. Mater. 26 (2014) 712–717.
[104] X. Xue, S. Jin, C. Zhang, K. Yang, S. Huo, F. Chen, G. Zou, X.J. Liang, Probe-inspired nano-prodrug with dual-color fluorogenic property reveals spatiotemporal drug release in living cells, ACS Nano 9 (2015) 2729–2739.
[105] W. Zhuang, Y. Xu, G. Li, J. Hu, B. Ma, T. Yu, X. Su, Y. Wang, Redox and pH dual-responsive polymeric micelles with aggregation-induced emission feature for cellular imaging and chemotherapy, ACS Appl. Mater. Interfaces 10 (2018) 18489–18498.
[106] X. He, Z. Zhao, L.H. Xiong, P.F. Gao, C. Peng, R.S. Li, Y. Xiong, Z. Li, H.H. Sung, I.D. Williams, Redox-active AIEgen derived plasmonic and fluorescent Core@shell nanoparticles for multimodality bioimaging, J. Am. Chem. Soc. (2018). https://doi.org/10.1021/jacs.1028b02350.
[107] Y. Zhao, R.T.K. Kwok, J.W.Y. Lam, B.Z. Tang, A highly fluorescent AIE-active theranostic agent with anti-tumor activity to specific cancer cells, Nanoscale 8 (2016) 12520–12523.
[108] Y. Chen, M. Li, Y. Hong, J.W.Y. Lam, Q. Zheng, B.Z. Tang, Dual-modal MRI contrast agent with aggregation-induced emission characteristic for liver specific imaging with long circulation lifetime, ACS Appl. Mater. Interfaces 6 (2014) 10783–10791.
[109] K.Y. Kim, H. Jin, J. Park, S.H. Jung, J.H. Lee, H. Park, S.K. Kim, J. Bae, J.H. Jung, Mitochondria-targeting self-assembled nanoparticles derived from triphenylphosphonium-conjugated cyanostilbene enable site-specific imaging and anticancer drug delivery, Nano Res. 11 (2018) 1082–1098.
[110] G. Feng, J.L.Y. Li, C. Claser, A. Balachander, Y. Tan, C.C. Goh, I.W.H. Kwok, L. Rénia, B.Z. Tang, L.G. Ng, B. Liu, Dual modal ultra-bright nanodots with aggregation-induced emission and gadolinium-chelation for vascular integrity and leakage detection, Biomaterials 152 (2018) 77–85.
[111] F. Xia, W. Fan, S. Jiang, Y. Ma, Y. Lu, J. Qi, E. Ahmad, X. Dong, W. Zhao, W. Wu, Size-dependent translocation of nanoemulsions via oral delivery, ACS Appl. Mater. Interfaces 9 (2017) 21660–21672.
[112] X. Hu, J. Zhang, Z. Yu, Y. Xie, H. He, J. Qi, X. Dong, Y. Lu, W. Zhao, W. Wu, Environment-responsive aza-BODIPY dyes quenching in water as potential probes to visualize the in vivo fate of lipid-based nanocarriers, Nanomed. Nanotechnol. Biol. Med. 11 (2015) 1939–1948.
[113] H. He, J. Zhang, Y. Xie, Y. Lu, J. Qi, E. Ahmad, X. Dong, W. Zhao, W. Wu, Bioimaging of intravenous polymeric micelles based on discrimination of integral particles using an environment-responsive probe, Mol. Pharm. 13 (2016) 4013–4019.
[114] H. Cao, Y. Yang, X. Chen, Z. Shao, Intelligent Janus nanoparticles for intracellular real-time monitoring of dual drug release, Nanoscale 8 (2016) 6754–6760.
[115] Y. Zhao, F. Fay, S. Hak, J. Manuel Perez-Aguilar, B.L. Sanchez-Gaytan, B. Goode, R. Duivenvoorden, C. de Lange Davies, A. Bjørkøy, H. Weinstein, Z.A. Fayad, C. Pérez-Medina, W.J.M. Mulder, Augmenting drug–carrier compatibility improves tumour nanotherapy efficacy, Nat. Commun. 7 (2016) 11221.
[116] N. Aibani, P.F. da Costa, J. Masterson, N. Marino, F.M. Raymo, J. Callan, B. Callan, The integration of triggered drug delivery with real time quantification using FRET; creating a super 'smart' drug delivery system, J. Control. Release 264 (2017) 136–144.
[117] A.L. Lainé, J. Gravier, M. Henry, L. Sancey, J. Béjaud, E. Pancani, M. Wiber, I. Texier, J.L. Coll, J.P. Benoit, C. Passirani, Conventional versus stealth lipid nanoparticles: formulation and in vivo fate prediction through FRET monitoring, J. Control. Release 188 (2014) 1–8.
[118] T.-G. Iversen, T. Skotland, K. Sandvig, Endocytosis and intracellular transport of nanoparticles: present knowledge and need for future studies, Nano Today 6 (2011) 176–185.
[119] M. Zhu, G. Nie, H. Meng, T. Xia, A. Nel, Y. Zhao, Physicochemical properties determine nanomaterial cellular uptake, transport, and fate, Acc. Chem. Res. 46 (2013) 622–631.
[120] L.Y.T. Chou, K. Ming, W.C.W. Chan, Strategies for the intracellular delivery of nanoparticles, Chem. Soc. Rev. 40 (2011) 233–245.
[121] G. Yu, T.R. Cook, Y. Li, X. Yan, D. Wu, L. Shao, J. Shen, G. Tang, F. Huang, X. Chen, P.J. Stang, Tetraphenylethene-based highly emissive metallacage as a component of theranostic supramolecular nanoparticles, Proc. Natl. Acad. Sci. 113 (2016) 13720–13725.
[122] W. Gao, D. Lee, Z. Meng, T. Li, Exploring intracellular fate of drug nanocrystals with crystal-integrated and environment-sensitive fluorophores, J. Control. Release 267 (2017) 214–222.
[123] C. Zhang, T. Zhang, S. Jin, X. Xue, X. Yang, N. Gong, J. Zhang, P.C. Wang, J.-H. Tian, J. Xing, X.-J. Liang, Virus-inspired self-assembled nanofibers with aggregation-induced emission for highly efficient and visible gene delivery, ACS Appl. Mater. Interfaces 9 (2017) 4425–4432.
[124] K.J. Cho, X. Wang, S.M. Nie, Z. Chen, D.M. Shin, Therapeutic nanoparticles for drug delivery in cancer, Clin. Cancer Res. 14 (2008) 1310–1316.
[125] M.B. Yatvin, J.N. Weinstein, W.H. Dennis, R. Blumenthal, Design of liposomes for enhanced local release of drugs by hyperthermia, Science 202 (1978) 1290–1293.
[126] T. Hoare, B.P. Timko, J. Santamaria, G.F. Goya, S. Irusta, S. Lau, C.F. Stefanescu, D.B. Lin, R. Langer, D.S. Kohane, Magnetically triggered nanocomposite membranes: a versatile platform for triggered drug release, Nano Lett. 11 (2011) 1395–1400.
[127] P. Moitra, K. Kumar, P. Kondaiah, S. Bhattacharya, Efficacious anticancer drug delivery mediated by a pH-sensitive self-assembly of a conserved tripeptide derived from tyrosine kinase NGF receptor, Angew. Chem. Int. Ed. 53 (2014) 1113–1117.
[128] S. Ganta, H. Devalapally, A. Shahiwala, M. Amiji, A review of stimuli-responsive nanocarriers for drug and gene delivery, J. Control. Release 126 (2008) 187–204.
[129] S. Mura, J. Nicolas, P. Couvreur, Stimuli-responsive nanocarriers for drug delivery, Nat. Mater. 12 (2013) 991–1003.
[130] A.T. Jones, M. Gumbleton, R. Duncan, Understanding endocytic pathways and intracellular trafficking: a prerequisite for effective design of advanced drug delivery systems, Adv. Drug Deliv. Rev. 55 (2003) 1353–1357.
[131] Q. Liu, X. Chen, J. Jia, W. Zhang, T. Yang, L. Wang, G. Ma, pH-Responsive poly(d,l-lactic-co-glycolic acid) nanoparticles with rapid antigen release behavior promote immune response, ACS Nano 9 (2015) 4925–4938.
[132] X. Xu, J. Wu, Y. Liu, M. Yu, L. Zhao, X. Zhu, S. Bhasin, Q. Li, E. Ha, J. Shi, C. Farokhzad Omid, Ultra-pH-responsive and tumor-penetrating nanoplatform for targeted siRNA delivery with robust anti-cancer efficacy, Angew. Chem. Int. Ed. 55 (2016) 7091–7094.
[133] Y. Ping, J. Guo, H. Ejima, X. Chen, J. Richardson Joseph, H. Sun, F. Caruso, pH-responsive capsules engineered from metal–phenolic networks for anticancer drug delivery, Small 11 (2015) 2032–2036.
[134] Y. Zhao, Z. Luo, M. Li, Q. Qu, X. Ma, S.H. Yu, Y. Zhao, A preloaded amorphous calcium carbonate/doxorubicin@Silica nanoreactor for pH-responsive delivery of an anticancer drug, Angew. Chem. Int. Ed. 54 (2014) 919–922.
[135] Y. Wang, Y. Deng, H. Luo, A. Zhu, H. Ke, H. Yang, H. Chen, Light-responsive nanoparticles for highly efficient cytoplasmic delivery of anticancer agents, ACS Nano 11 (2017) 12134–12144.
[136] W.-L. Chiang, T.-T. Lin, R. Sureshbabu, W.-T. Chia, H.-C. Hsiao, H.-Y. Liu, C.-M. Yang, H.-W. Sung, A rapid drug release system with a NIR light-activated molecular switch for dual-modality photothermal/antibiotic treatments of subcutaneous abscesses, J. Control. Release 199 (2015) 53–62.
[137] C. Yao, P. Wang, X. Li, X. Hu, J. Hou, L. Wang, F. Zhang, Near-infrared-triggered azobenzene-liposome/upconversion nanoparticle hybrid vesicles for remotely controlled drug delivery to overcome cancer multidrug resistance, Adv. Mater. 28 (2016) 9341–9348.
[138] A.M. Goodman, O. Neumann, K. Nørregaard, L. Henderson, M.-R. Choi, S.E. Clare, N.J. Halas, Near-infrared remotely triggered drug-release strategies for cancer treatment, Proc. Natl. Acad. Sci. 114 (2017) 12419–12424.
[139] H. Yan, C. Teh, S. Sreejith, L. Zhu, A. Kwok, W. Fang, X. Ma, T. Nguyen Kim, V. Korzh, Y. Zhao, Functional mesoporous silica nanoparticles for photothermal-controlled drug delivery in vivo, Angew. Chem. Int. Ed. 124 (2012) 8498–8502.
[140] R. Tong, H.D. Hemmati, R. Langer, D.S. Kohane, Photoswitchable nanoparticles for triggered tissue penetration and drug delivery, J. Am. Chem. Soc. 134 (2012) 8848–8855.
[141] Y.T. Chang, P.Y. Liao, H.S. Sheu, Y.J. Tseng, F.Y. Cheng, C.S. Yeh, Near-infrared light-responsive intracellular drug and siRNA release using au nanoensembles with oligonucleotide-capped silica shell, Adv. Mater. 24 (2012) 3309–3314.
[142] K. Han, Q. Lei, H.Z. Jia, S.B. Wang, W.N. Yin, W.H. Chen, S.X. Cheng, X.Z. Zhang, A tumor targeted chimeric peptide for synergistic endosomal escape and therapy by dual-stage light manipulation, Adv. Funct. Mater. 25 (2015) 1248–1257.
[143] L. Dai, Y. Yu, Z. Luo, M. Li, W. Chen, X. Shen, F. Chen, Q. Sun, Q. Zhang, H. Gu, K. Cai, Photosensitizer enhanced disassembly of amphiphilic micelle for ROS-response targeted tumor therapy in vivo, Biomaterials 104 (2016) 1–17.
[144] Y.Y. Yuan, S.D. Xu, C.J. Zhang, B. Liu, Light-responsive AIE nanoparticles with cytosolic drug release to overcome drug resistance in cancer cells, Polym. Chem. 7 (2016) 3530–3539.
[145] T. Nomoto, S. Fukushima, M. Kumagai, K. Machitani, Y. Matsumoto Arnida, M. Oba, K. Miyata, K. Osada, N. Nishiyama, K. Kataoka, Three-layered polyplex micelle as a multifunctional nanocarrier platform for light-induced systemic gene transfer, Nat. Commun. 5 (2014) 3545–3554.

[146] Y.Y. Yuan, C.J. Zhang, B. Liu, A photoactivatable AIE polymer for light-controlled gene delivery: concurrent endo/lysosomal escape and DNA unpacking, Angew. Chem. Int. Ed. 54 (2015) 11419–11423.
[147] S.H. Lee, M.K. Gupta, J.B. Bang, H. Bae, H.J. Sung, Current progress in reactive oxygen species (ROS)-responsive materials for biomedical applications, Adv. Healthc. Mater. 2 (2013) 908–915.
[148] D. Fischer, T. Bieber, Y.X. Li, H.P. Elsasser, T. Kissel, A novel non-viral vector for DNA delivery based on low molecular weight, branched polyethylenimine: effect of molecular weight on transfection efficiency and cytotoxicity, Pharm. Res. 16 (1999) 1273–1279.
[149] Q. Zhang, C. Shen, N. Zhao, F.J. Xu, Redox-responsive and drug-embedded silica nanoparticles with unique self-destruction features for efficient gene/drug codelivery, Adv. Funct. Mater. 27 (2017) 1606229–1606240.
[150] Y. Tu, F. Peng, B. White Paul, A. Wilson Daniela, Redox-sensitive stomatocyte nanomotors: destruction and drug release in the presence of glutathione, Angew. Chem. Int. Ed. 129 (2017) 7728–7732.
[151] Z. Deng, S. Yuan, X. Xu Ronald, H. Liang, S. Liu, Reduction-triggered transformation of disulfide-containing micelles at chemically tunable rates, Angew. Chem. Int. Ed. (2018). https://doi.org/10.1002/anie.201802909.
[152] J. Hu, W. Zhuang, B. Ma, X. Su, T. Yu, G. Li, Y. Hu, Y. Wang, Redox-responsive biomimetic polymeric micelle for simultaneous anticancer drug delivery and aggregation-induced emission active imaging, Bioconjug. Chem. 29 (2018) 1897–1910.
[153] Y.-F. Wang, L. Liu, X. Xue, X.-J. Liang, Nanoparticle-based drug delivery systems: What can they really do in vivo? F1000Research 6 (2017) 681–688.
[154] S. Han, A. Samanta, X. Xie, L. Huang, J. Peng, J. Park Sung, L. Teh Daniel Boon, Y. Choi, Y.-T. Chang, H. All Angelo, Y. Yang, B. Xing, X. Liu, Gold and hairpin DNA functionalization of upconversion nanocrystals for imaging and in vivo drug delivery, Adv. Mater. 29 (2017) 1700244–1700250.
[155] Y. Lyu, Y. Fang, Q. Miao, X. Zhen, D. Ding, K. Pu, Intraparticle molecular orbital engineering of semiconducting polymer nanoparticles as amplified theranostics for in vivo photoacoustic imaging and photothermal therapy, ACS Nano 10 (2016) 4472–4481.
[156] J. Liu, J. Bu, W. Bu, S. Zhang, L. Pan, W. Fan, F. Chen, L. Zhou, W. Peng, K. Zhao, J. Du, J. Shi, Real-time in vivo quantitative monitoring of drug release by dual-mode magnetic resonance and upconverted luminescence imaging, Angew. Chem. Int. Ed. 53 (2014) 4551–4555.
[157] R. Zhang, Q. Fan, M. Yang, K. Cheng, X. Lu, L. Zhang, W. Huang, Z. Cheng, Engineering melanin nanoparticles as an efficient drug–delivery system for imaging-guided chemotherapy, Adv. Mater. 27 (2015) 5063–5069.
[158] F. Andre, L. Pusztai, Molecular classification of breast cancer: implications for selection of adjuvant chemotherapy, Nat. Clin. Pract. Oncol. 3 (2006) 621–632.
[159] D. Zardavas, A. Irrthum, C. Swanton, M. Piccart, Clinical management of breast cancer heterogeneity, Nat. Rev. Clin. Oncol. 12 (2015) 381–394.
[160] S.S. Liow, Q. Dou, D. Kai, Z. Li, S. Sugiarto, C.Y.Y. Yu, R.T.K. Kwok, X. Chen, Y.L. Wu, S.T. Ong, A. Kizhakeyil, N.K. Verma, B.Z. Tang, X.J. Loh, Long-term real-time in vivo drug release monitoring with AIE thermogelling polymer, Small 13 (2017) 1603404–1603411.
[161] T.J. Dougherty, C.J. Gomer, B.W. Henderson, G. Jori, D. Kessel, M. Korbelik, J. Moan, Q. Peng, Photodynamic therapy, J. Natl. Cancer Inst. 90 (1998) 889–905.
[162] K. Kalka, H. Merk, H. Mukhtar, Photodynamic therapy in dermatology, J. Am. Acad. Dermatol. 42 (2000) 389–413.
[163] T.A. A, A. Akira, M. Koji, S. Frank, S. Anton, W. Chen-Ying, K. Geena, R. George, I. Isao, I. Yuichi, Application of antimicrobial photodynamic therapy in periodontal and peri-implant diseases, Periodontology 51 (2009) 109–140.
[164] M. Li, Y. Gao, Y. Yuan, Y. Wu, Z. Song, B.Z. Tang, B. Liu, Q.C. Zheng, One-step formulation of targeted aggregation-induced emission dots for image-guided photodynamic therapy of cholangiocarcinoma, ACS Nano 11 (2017) 3922–3932.
[165] D. Ding, K. Li, B. Liu, B.Z. Tang, Bioprobes based on AIE fluorogens, Acc. Chem. Res. 46 (2013) 2441–2453.
[166] J. Zhang, C. Li, X. Zhang, S. Huo, S. Jin, F.-F. An, X. Wang, X. Xue, C.I. Okeke, G. Duan, F. Guo, X. Zhang, J. Hao, P.C. Wang, J. Zhang, X.-J. Liang, In vivo tumor-targeted dual-modal fluorescence/CT imaging using a nanoprobe co-loaded with an aggregation-induced emission dye and gold nanoparticles, Biomaterials 42 (2015) 103–111.
[167] C.Y. Yu, H. Xu, S. Ji, R.T. Kwok, J.W. Lam, X. Li, S. Krishnan, D. Ding, B.Z. Tang, Mitochondrion-anchoring photosensitizer with aggregation-induced emission characteristics synergistically boosts the radiosensitivity of cancer cells to ionizing radiation, Adv. Mater. 29 (2017) 1606167.